MECHANICS OF ADVANCED MATERIALS AND STRUCTURES
2016, VOL. 0, NO. 0, 1–20
http://dx.doi.org/10.1080/15376494.2016.1194505

Taylor & Francis
Taylor & Francis Group

ORIGINAL ARTICLE

Stretching and bending deformations due to normal and shear tractions of doubly curved shells using third-order shear and normal deformable theory

P. H. Shah and R. C. Batra

Department of Biomedical Engineering and Mechanics, Virginia Polytechnic Institute and State University, Blacksburg, Virginia, USA

ABSTRACT

We analyze static infinitesimal deformations of doubly curved shells using a third-order shear and normal deformable theory (TSNDT) and delineate effects of the curvilinear length/thickness ratio, R/a, a/h, radius of curvature/curvilinear length and the ratio of the two principal radii on through-the-thickness stresses, strain energies of the in-plane and the transverse shear and normal deformations, and strain energies of stretching and bending deformations for loads that include uniform normal tractions on a major surface and equal and opposite tangential tractions on the two major surfaces. In the TSNDT the three displacement components at a point are represented as complete polynomials of degree three in the thickness coordinate. Advantages of the TSNDT include not needing a shear correction factor, allowing stresses for monolithic shells to be computed from the constitutive relation and the shell theory displacements, and considering general tractions on bounding surfaces. For laminated shells we use an equivalent single layer TSNDT and find the in-plane stresses from the constitutive relations and the transverse stresses with a one-step stress recovery scheme. The in-house developed finite element software is first verified by comparing displacements and stresses in the shell computed from it with those from either analytical or numerical solutions of the corresponding 3D problems. The strain energy of a spherical shell is found to approach that of a plate when R/*a* exceeds 10. For a thick clamped shell of aspect ratio 5 subjected to uniform normal traction on the outer surface, the in-plane and the transverse deformations contribute equally to the total strain energy for R/*a* greater than 5. However, for a cantilever shell of aspect ratio 5 subjected to equal and opposite uniform tangential tractions on the two major surfaces, the strain energy of in-plane deformations equals 95–98% of the total strain energy. Numerical results presented herein for several problems provide insights into different deformation modes, help designers decide when to consider effects of transverse deformations, and use the TSNDT for optimizing doubly curved shells.

ARTICLE HISTORY
Received 30 December 2015
Accepted 12 May 2016

KEYWORDS
Bending and stretching deformations; doubly curved laminated shells; strain energy; TSNDT

1. Introduction

Laminated composite shells are widely used in aircraft, aerospace, marine, automobile, power generation, and chemical industries. A shell is called shallow (deep) if its rise equals at most (at least) one-fifth of its smallest planform dimension [1]. A shell is termed thick, moderately thick, and thin if the ratio of the smallest curvilinear length and/or the smallest radius of curvature to the thickness is, respectively, at most 10, between 10 and 20, and at least 20 [1].

For thin shallow shells, classical theories, such as Love's first approximation theory (LFAT) [2], Donnell's [3], Sanders' [4], and Flügge's [5] shell theories, among others, accurately predict their mechanical deformations. The LFAT is based on the following postulates: (i) the shell is thin and shallow, (ii) displacements and displacement gradients are infinitesimal, (iii) the transverse normal stress is negligible, (iv) a normal to the mid-surface stays normal to it during the deformation process, and (v) the shell thickness, h, does not change. It is assumed that $h/R << 1$ and, hence, terms z/R_1 and z/R_2 are $<<1$, where z is the thickness coordinate with the origin at the shell's mid-surface, and R_1 and R_2 are the principal radii of curvature. Postulates (iv) and (v) imply that the transverse shear and the transverse normal strains vanish. Donnell's [3], Sanders' [4], and Flügge's [5] shell theories are also based on the above five hypotheses. However, they use different approximations for strains and the shell curvatures. Donnell's theory [3] neglects gradients of in-plane displacements in expressions for the shell curvatures. This makes the theory inconsistent with respect to rigid body motions. For example, Kraus [6] showed that when a rigid body rotation is applied to a nonspherical curved shell or an unsymmetrically loaded shell of revolution, torsion is induced in the shell. In Sander's theory [4], expressions for shell curvatures are modified to ensure that a rigid body motion does not induce strains in the shell. Flügge [5] expanded the terms $1/(1 + z/R_i)$ $(i = 1, 2)$ appearing in expressions of strains as binomial series and retained terms up to second order in z/R_i.

For thick and moderately thick shells, transverse deformations may become significant, in which case classical theories will not provide accurate responses. Reissner [7] pointed out in 1947 that for sandwich shells with $(tE_f)/(hE_c) >> 1$ both transverse shear and transverse normal deformations should be considered. Here, t and E_f (h and E_c) equal, respectively, the thickness and the longitudinal modulus of the face sheet (core).

CONTACT R. C. Batra rbatra@vt.edu Department of Biomedical Engineering and Mechanics, Virginia Polytechnic Institute and State University, 333E Norris Hall, M/C 0219, Blacksburg, VA 24061.
Color versions of one or more of the figures in this article are available online at www.tandfonline.com/umcm.

Reissner developed a theory with each face sheet modeled as a membrane and the core as a 3-dimensional (3D) continuum. For laminates with a sinusoidal pressure of amplitude q applied on the top surface, Vel and Batra [8] found that the average transverse normal strain near a traction free edge is of the order of q/E, where E equals Young's modulus in the fiber direction.

The first-order shear deformation theory (FSDT) assumes constant transverse shear strains across the shell thickness, and an appropriate shear correction factor is used to account for nonuniform through-the-thickness shear strains. Higher-order shear deformation theories [9–13] do not require a shear correction factor. Reddy and Liu [11], Liew and Lim [12], and Xiao-Ping [13] developed third-order shear deformation theories (TSDTs) for analyzing shells' deformations in which the in-plane displacements are expressed as complete polynomials of degree three and the transverse normal displacement is assumed to be constant across the shell thickness. This leads to a parabolic distribution of transverse shear strains through the thickness and zero transverse normal strain. The number of independent unknowns involved in these theories is reduced to that for the FSDT by requiring that transverse shear stresses vanish on the major surfaces of the shell. Xio-Ping [13] incorporated Love's first-order geometric approximation and Donnell's simplification.

Shell theories accounting for transverse shear and normal deformations have been developed, among others, by Hildebrand et al. [14], Reissner [15], and Whitney and Sun [16, 17]. Bert [18], Leissa [19], Qatu [1, 20], and Liew et al. [21], among others, have reviewed shell theories. For a complete list of papers on shells, the reader should see the website www.shellbuckling.com developed and regularly updated by Dr. David Bushnell.

For analyzing deformations of laminated shells, either an equivalent single layer (ESL) or a layer-wise (LW) shell theory is often employed. In the ESL (LW) theory the number of unknowns is the same as (number of layers times) that for a monolithic shell. Thus, a LW theory is computationally more expensive than an ESL theory. However, in an ESL theory the transverse normal and the transverse shear stresses obtained from constitutive relations and the shell theory displacements are generally not accurate and may not satisfy traction continuity conditions across interfaces between adjoining layers and traction boundary conditions on major surfaces. These stresses computed using a stress recovery scheme (SRS), which usually involves integration of the 3D equilibrium equations along the thickness direction by starting from a major surface of the shell, are reasonably accurate. Different ESL and LW thin and thick plate/shell theories have been reviewed by Carrera [22], Ambartsumian [23, 24], Reddy [25], Reddy and Arciniega [26], and Kapania [27].

The SRS described above is a one-step method [28] and has been employed by Pagano [29] and Rohwer [30], among others. It is possible that tractions on the top surface computed using this scheme starting from the bottom surface do not satisfy the applied surface tractions there. This difference can be used to measure error in the numerical solution. Tornabene et al. [31] employed the Murakami function for satisfying the traction boundary condition on the top surface. The two-step methods, such as those employed by Noor et al. [32, 33] and Malik and Noor [34], use iterative techniques to compute the transverse stresses and satisfy traction boundary conditions at both major surfaces. Rohwer et al. [28] and Kant and Swaminathan [35] have reviewed different methods to estimate interlaminar transverse stresses. The state-space approach used by Tarn and Wang [36] is a one-step method and simultaneously integrates along the thickness direction the three displacement components and the three transverse stresses.

Vidoli and Batra [37] and Batra and Vidoli [38] deduced a variable order plate theory for piezoelectric and orthotropic linear elastic plates in which the order K up to which terms in the thickness coordinate, z, are kept is a variable. They called the plate theory "mixed" ("compatible") when the constitutive relations for the plate are derived from the Hellinger–Prange–Reissner principle (from the plate theory displacement field and the constitutive relation of the 3D linear elasticity theory [LET]). The mixed theory exactly satisfies traction boundary conditions specified on the two major surfaces of the plate. Batra and Vidoli [38] showed that for a thick beam results from the mixed plate theory are in better agreement with the LET solutions than those from the compatible theory of the same order. Qian et al. [39] and Batra and Aimmanee [40] have used the compatible (mixed) theory of different orders to show that in-plane modes of free vibration in a thick plate are well captured when $K = 3$. Qian and Batra [41] have extended the compatible theory to analyze thermo-elastic deformations. Batra and Xiao [42] have shown that a LW compatible third-order shear and normal deformation theory (TSNDT) gives stresses in curved laminated beams that agree well with those obtained by using the LET. Using the TSNDT, Shah and Batra [43] found that for a monolithic clamped square plate loaded with a uniform normal traction on a major surface, the strain energy of transverse shear deformations can be about 7% (20%) of the total strain energy of deformations for aspect ratio (i.e., length/thickness) of 20 (10), and can be as high as 50% for an aspect ratio of 5.

In order to optimally design a doubly curved shell for a given application, it is important to understand how geometric parameters (e.g., ratio of two principal radii, ratio of the maximum principal radius of curvature to the curvilinear length, curvilinear length/thickness) affect its deformations. Shi et al. [44] investigated the effect of the ratio of two principal radii of curvature on frequencies of free vibration of monolithic isotropic doubly curved shells using the LFAT. They found that natural frequencies increase with an increase in the R_2/R_1 ratio for a given R_2/l_2 ratio and decrease with an increase in the R_2/l_2 ratio for a given R_2/R_1 ratio, where l_1 and l_2 are the two planform lengths. Fan and Zhang [45], Wu et al. [46], and Huang et al. [47] computed analytical solutions for static deformations of laminated doubly curved shells and reported the centroidal displacement of shells for different curvatures. They found that the displacement decreases with an increase in the curvature for a fixed aspect ratio. The former two studies used the 3D LET and the latter used a higher-order shear deformation theory (HSDT). For a monolithic isotropic cylindrical shell, Calladine [48] derived an expression relating the geometric parameters of the shell and the ratio of stretching and bending stiffnesses. Kalnins [49] studied free vibrations of monolithic isotropic spherical shells using classical bending theory and computed strain energies due to bending and stretching for each mode. He identified the vibration mode as bending (stretching) if the strain energy

due to bending (stretching) is larger than that due to stretching (bending). He found that frequencies of stretching modes are independent of the shell thickness but those of bending modes increase with the thickness, and the frequency of the first stretching mode is relatively high compared to that of the first bending mode. We could not find works describing the effect of geometric parameters on strain energies of various deformation modes for doubly curved shells deformed under external loads. This knowledge can help structural designers identify significant deformation modes for given loading conditions and optimize geometric parameters of the shell.

Here, we study infinitesimal deformations of doubly curved shells deformed statically with arbitrary surface tractions applied on their major surfaces using the compatible TSNDT and the finite element method (FEM) to numerically solve several problems using in-house developed software. For laminated shells, we use an ESL and one-step SRS to compute stresses. First, we study for various values of length/thickness and (radius of curvature)/length ratios deformations of doubly curved laminated shells and compare results from the TSNDT with the corresponding analytical 3D LET solutions available in the literature. Next, we study three example problems for a monolithic doubly curved shell subjected to (i) a uniform normal traction on one of the major surfaces, (ii) combined normal and tangential tractions on a major surface, and (iii) equal and opposite tangential tractions on the two major surfaces. For most of these problems we delineate effects of geometric parameters on stresses, and strain energies of bending and stretching deformations and of in-plane and transverse deformations, and compare predictions from the TSNDT with those from the solutions of the 3D LET equations.

2. Formulation of the problem

We analyze static infinitesimal deformations of a laminated doubly curved shell schematically shown in Figure 1. The shell is composed of N layers of not necessarily equal thickness. Each layer is made of a homogeneous, orthotropic, and linear elastic material with adjacent layers perfectly bonded to each other. The orthogonal curvilinear coordinates (y_1, y_2, y_3) are such that $y_1 =$ constant and $y_2 =$ constant are curves of principal curvature on the mid-surface, $y_3 = 0$. The position vectors of a point with respect to the fixed rectangular Cartesian coordinate axes (X_1, X_2, X_3) and (x_1, x_2, x_3) with the X_3- and the x_3-axes parallel to the y_3-axis are denoted by $\mathbf{X}$ and $\mathbf{x}$ in the reference and the current configurations, respectively. We denote the total thickness and the constant principal radii of curvature of the mid-surface of the shell by h, R_{1m}, and R_{2m}, respectively, the arc lengths of the shell mid-surface in the y_1- and the y_2-directions by a and b, respectively, and the corresponding planform lengths by l_1 and l_2, respectively.

Components G_{ij} of the metric tensor in the reference configuration are given by:

$$G_{ij} = \mathbf{A_i} \cdot \mathbf{A_j}, \quad \mathbf{A_i} = \frac{\partial \mathbf{X}}{\partial y_i} \quad (i = 1,\ 2,\ 3), \tag{1}$$

where $\mathbf{A_i} \cdot \mathbf{A_j}$ equals the inner product between vectors $\mathbf{A_i}$ and $\mathbf{A_j}$. We note that for the orthogonal curvilinear coordinate system, G_{ij} is nonzero only when i = j. The unit base vectors $(\bar{\mathbf{e}}_1,\ \bar{\mathbf{e}}_2,\ \bar{\mathbf{e}}_3)$ associated with the curvilinear coordinate axes (y_1, y_2, y_3) are $\bar{\mathbf{e}}_i = \frac{\mathbf{A}_{(i)}}{H_{(i)}}$ (no sum on i), where $H_1 = (1+\frac{y_3}{R_1})$, $H_2 = (1+\frac{y_3}{R_2})$, $H_3 = 1$, and R_1 and R_2 are radii of curvature at the point (y_1, y_2, y_3).

The displacement $\mathbf{u}$ of a point is given by $\mathbf{u} = \mathbf{x} - \mathbf{X}$. The physical components of the infinitesimal strain tensor in the curvilinear coordinate system are given by [50]:

$$\begin{aligned}
&\epsilon_{11} = \frac{1}{H_1}\left(\frac{\partial u_1}{\partial y_1} + \frac{u_3}{R_1}\right), \quad \epsilon_{22} = \frac{1}{H_2}\left(\frac{\partial u_2}{\partial y_2} + \frac{u_3}{R_2}\right),\\
&2\epsilon_{12} = \frac{1}{H_1}\frac{\partial u_2}{\partial y_1} + \frac{1}{H_2}\frac{\partial u_1}{\partial y_2},\\
&2\epsilon_{13} = \frac{1}{H_1}\left(\frac{\partial u_3}{\partial y_1} - \frac{u_1}{R_1}\right) + \frac{\partial u_1}{\partial y_3},\\
&2\epsilon_{23} = \frac{1}{H_2}\left(\frac{\partial u_3}{\partial y_2} - \frac{u_2}{R_2}\right) + \frac{\partial u_2}{\partial y_3}, \quad \epsilon_{33} = \frac{\partial u_3}{\partial y_3},
\end{aligned} \tag{2}$$

where ϵ_{ii} (i = 1, 2, 3) is the normal strain along the y_i-direction, ϵ_{12} is the in-plane shear strain, and ϵ_{13} and ϵ_{23} are the transverse shear strains.

In the TSNDT, the displacement, u_i, at a point is expressed as a complete polynomial of degree 3 in the thickness coordinate, y_3:

$$\mathbf{d}(y_1, y_2, y_3) = (y_3)^i\, \mathbf{d_i}(y_1, y_2), \quad (i = 0,\ 1,\ 2,\ 3). \tag{3}$$

Unless stated otherwise, a repeated index implies summation over the range of the index. In Eq. (3):

$$\mathbf{d} = [u_1\ u_2\ u_3]^{\mathbf{T}} \text{ and } \mathbf{d_i} = [u_{1i}\ u_{2i}\ u_{3i}]^{\mathbf{T}} \quad (i = 0,\ 1,\ 2,\ 3), \tag{3.1}$$

where $u_{i0} = u_i(y_1, y_2, 0)$ (i = 1, 2, 3). One interpretation of variables is:

$$\begin{aligned}
&u_{i1} = \left.\frac{\partial u_i}{\partial y_3}\right|_{y_3=0}, 2u_{i2} = \left.\frac{\partial^2 u_i}{\partial (y_3)^2}\right|_{y_3=0},\\
&6u_{i3} = \left.\frac{\partial^3 u_i}{\partial (y_3)^3}\right|_{y_3=0} \quad (i = 1,\ 2,\ 3).
\end{aligned} \tag{3.2}$$

The 12D vector $\bar{\mathbf{d}} = [\mathbf{d_0}, \mathbf{d_1}, \mathbf{d_2}, \mathbf{d_3}]$ is referred to as the vector of generalized displacements at a point on the shell's mid-surface. We substitute for u_i from Eq. (3) into Eq. (2) to obtain:

$$\epsilon = \mathbf{Z_i}(y_3)\, \mathbf{L}\mathbf{d_i}(y_1,\ y_2) \quad (i = 0,\ 1,\ 2,\ 3), \tag{4}$$

where

$$\epsilon = [\epsilon_{11}\ \epsilon_{22}\ \epsilon_{33}\ 2\epsilon_{23}\ 2\epsilon_{13}\ 2\epsilon_{12}]^{\mathbf{T}}, \tag{4.1}$$

and matrices $\mathbf{Z_i}$ (i = 0, 1, 2, 3) and the operator matrix $\mathbf{L}$ are defined in Appendix A, respectively, by Eqs. (A.1) and (A.2).

Similar to components of the strain tensor, we write components of the Cauchy stress tensor as a 6D vector:

$$\boldsymbol{\sigma} = [\sigma_{11}\ \sigma_{22}\ \sigma_{33}\ \sigma_{23}\ \sigma_{13}\ \sigma_{12}]^{\mathrm{T}}. \tag{5}$$

The constitutive relation (Hooke's law) for a linear elastic material is:

$$\begin{aligned}
&\sigma_{ij} = C_{ijmn}\epsilon_{mn}, \quad C_{ijmn} = C_{mnij} = C_{jimn},\\
&(i,\ j,\ m,\ n = 1,\ 2,\ 3),
\end{aligned} \tag{6}$$

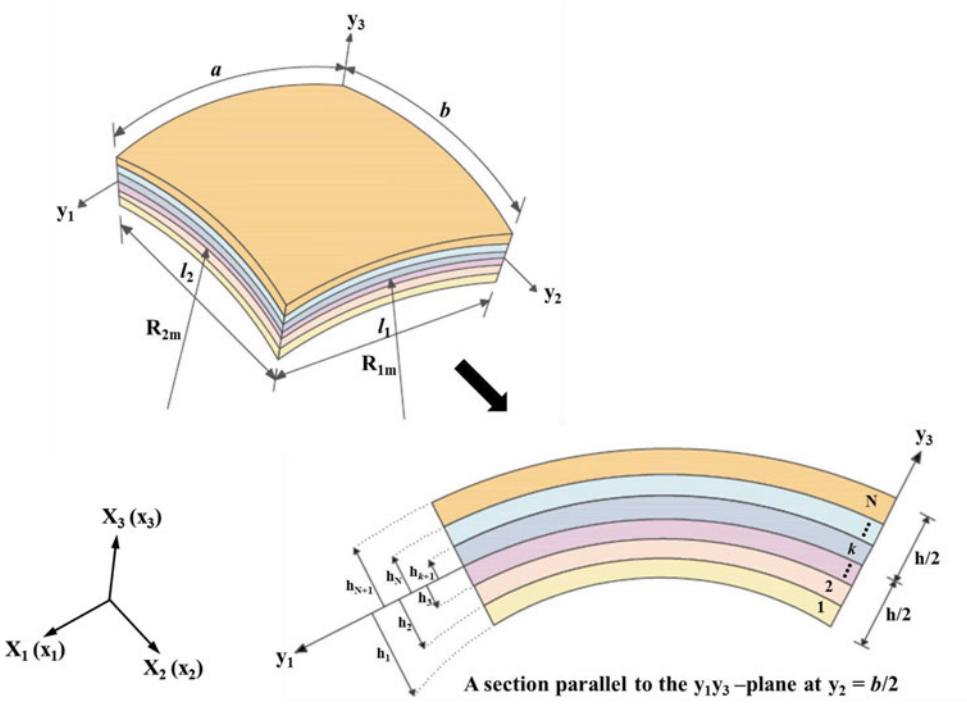

Figure 1. Geometry and coordinate system of a doubly curved laminated shell.

where $\boldsymbol{C}$ is the fourth-order elasticity tensor having 21 independent components for a general anisotropic material. For an orthotropic, a transversely isotropic, and an isotropic material, the independent components of C reduce, respectively, to 9, 5, and 2.

With respect to the material principal axes, Eq. (6) for an orthotropic material of layer k becomes:

$$\begin{Bmatrix} \sigma_{11}^k \\ \sigma_{22}^k \\ \sigma_{33}^k \\ \sigma_{23}^k \\ \sigma_{13}^k \\ \sigma_{12}^k \end{Bmatrix} = \begin{bmatrix} C_{1111}^k & C_{1122}^k & C_{1133}^k & 0 & 0 & 0 \\ C_{1122}^k & C_{2222}^k & C_{2233}^k & 0 & 0 & 0 \\ C_{1133}^k & C_{2233}^k & C_{3333}^k & 0 & 0 & 0 \\ 0 & 0 & 0 & C_{2323}^k & 0 & 0 \\ 0 & 0 & 0 & 0 & C_{1313}^k & 0 \\ 0 & 0 & 0 & 0 & 0 & C_{1212}^k \end{bmatrix} \times \begin{Bmatrix} \in_{11}^k \\ \in_{22}^k \\ \in_{33}^k \\ 2 \in_{23}^k \\ 2 \in_{13}^k \\ 2 \in_{12}^k \end{Bmatrix}, \tag{7}$$

where quantities for the kth layer are indicated by the superscript k. In the global coordinate axes (y_1, y_2, y_3) C_{ijmn} are computed by using the tensor transformation rules for the stress and the strain tensors, and the 6×6 matrix may be fully populated; e.g., see [26]. For the TSNDT, elastic constants in Eq. (7) are the same as those used in the LET, i.e., they are not modified to satisfy $\sigma_{33} = 0$ as is often done in the LFAT.

We use the principle of minimum potential energy to derive equations governing static deformations of the shell:

$$\delta\Pi = \delta\,(\mathrm{W} - \mathrm{W_f}) = 0, \tag{8}$$

where δ is the variational operator, Π is the potential energy of the shell, and W and $\mathrm{W_f}$ are, respectively, the strain energy of deformation and the work done by the external force in the absence of body forces given by:

$$\mathrm{W} = \frac{1}{2}\sum_{k=1}^{\mathrm{N}} \int_{\Omega^k} (\boldsymbol{\epsilon}^k)^{\mathrm{T}} \boldsymbol{\sigma}^k \, \mathrm{d}\Omega^k, \tag{8.1}$$

$$\mathrm{W_f} = \int_{\bar{\mathrm{A}}} \mathbf{d}^{\mathrm{T}} \bar{\mathbf{f}} \, \mathrm{d}\bar{\mathrm{A}}. \tag{8.2}$$

Here Ω^k is the region occupied by the kth layer in the reference configuration, and $\bar{\mathrm{A}}$ is the part of the bounding surface of the shell on which surface traction, $\bar{\mathbf{f}}$, is specified. Points on the remainder of the boundary of the domain, Ω, occupied by the shell have either null tractions (i.e., are on a free surface) or have displacements prescribed on them. The work done by reaction forces at points of the boundary where displacements are prescribed is not included in Eq. (8) because variations in the prescribed displacements are null.

We substitute in Eq. (8.1) for $\boldsymbol{\sigma}^k$ in terms of $\boldsymbol{\epsilon}^k$ from Eq. (7), and substitute for $\boldsymbol{\epsilon}^k$ in terms of the generalized displacements defined on the mid-surface of the shell from Eq. (4). Also, we substitute in Eq. (8.2) for $\mathbf{d}$ in terms of $\mathbf{d_i}$ (i = 0, 1, 2, 3) from Eq. (3). In the resulting expression for $\delta\Pi$, we integrate with respect to y_3 over the shell thickness to obtain an integral equation for $\delta\Pi$ with the integrand defined on the mid-surface.

The mid-surface of the shell is discretized into a finite element (FE) mesh of disjoint 8-node iso-parametric quadrilateral elements. Thus $\delta\Pi$ equals the sum of integrals over each element. Following the standard procedure (e.g., see [43] or Appendix B) we obtain equations governing static deformations of the shell as

$$\mathbf{KU} = \mathbf{F}. \tag{9}$$

Table 1. Nomenclature for boundary conditions specified at $y_1 = 0$ or a.

Notation	Type	BCs in the 3D LET	BCs in the TSNDT
C	Clamped	$u_1 = 0,\ u_2 = 0,\ u_3 = 0$	$u_{1i} = 0,\ u_{2i} = 0,\ u_{3i} = 0$
S	Simply supported	$\sigma_{11} = 0,\ u_2 = 0,\ u_3 = 0$	$M^i_{11} = 0,\ u_{2i} = 0,\ u_{3i} = 0$
F	Traction free	$\sigma_{11} = 0,\ \sigma_{12} = 0,\ \sigma_{13} = 0$	$M^i_{11} = 0,\ M^i_{12} = 0,\ M^i_{13} = 0$

In Eq. (9) **K** is the global stiffness matrix, **U** the global vector of generalized nodal displacements, and **F** the global load vector; their expressions are given by Eq. (B.10) in Appendix B. The vector **F** of generalized forces at nodes is work equivalent to surface tractions applied on the bounding surfaces of the shell. For a FE mesh of N_{node} nodes, before applying essential boundary conditions, the length of vector **U** equals $(12\ N_{node})$ since a node has 12 degrees of freedom.

We consider three types of boundary conditions (BCs) specified at a point on a shell edge. For example, at the edges $y_1 = 0$ and a, definitions of these BCs in the 3D LET and their equivalence in terms of variables of the TSNDT are listed in Table 1.

In Table 1, the index i takes values 0, 1, 2, and 3, and

$$M^i_{1n} = \int_{-h/2}^{h/2} (y_3)^i \sigma_{1n} dy_3, \quad (n = 1, 2, 3)\,. \tag{10}$$

The displacement (or essential) boundary conditions applied at points on a shell edge are satisfied while solving algebraic equations (9).

3. Example problems

When presenting and discussing below results for several problems, we use the more common notation and replace (X_1, X_2, X_3) and (u_1, u_2, u_3) by (x, y, z) and (u, v, w), respectively. We compare numerical results computed using the TSNDT with the corresponding 3D LET solutions obtained by either analytical methods or the FEM with the commercial software, ABAQUS. Unless mentioned otherwise, the 3D FE results are obtained using a uniform mesh of 8-node brick elements with 100 elements along the x- and the y-directions and 10 elements in the thickness direction, which corresponds to 336,633 nodal degrees of freedom (DoF).

We compute stresses from the constitutive relation and the shell theory displacements. For laminated shells we find in-plane stresses (σ_{xx}, σ_{yy}, σ_{xy}) from the constitutive relations and the shell theory displacements, and compute transverse stresses (σ_{xz}, σ_{yz}, σ_{zz}) by using the one-step SRS; these are indicated below by labels "C" and "SRS," respectively. We note that the in-plane stresses in a FE are evaluated at 3×3 quadrature points and by fitting to them a complete quadratic polynomial by the least squares method, stresses and their derivatives with respect to x and y at any point in the FE are computed.

3.1. *Convergence of the solution with FE mesh refinement*

We consider a 0°/90°/0° orthotropic laminated spherical shell ($R_{1m} = R_{2m} = R$) with $a = b$, $R/a = 2$, h = 10 mm, and $a/h = 10$, only the outer surface subjected to a uniform normal tensile traction, q_0, and assign following values to material parameters:

$$E_1 = 172.4\ \text{GPa},\ E_1/E_2 = 25,\ E_3 = E_2,\ G_{12} = G_{13} = 0.5E_2,$$

$$G_{23} = 0.2E_2,\ \nu_{12} = \nu_{13} = \nu_{23} = 0.25.$$

Here, E_1 denotes Young's modulus along the Z_1 axis, and $G_{12}(\nu_{12})$ the shear modulus (Poisson's ratio) in the Z_1Z_2-plane where the Z_1-, the Z_2-, and the Z_3- are the material principal axes. Values of elastic constants with respect to global coordinate axes are obtained by using the tensor transformation rules.

The lamination scheme, $\alpha_1/\alpha_2/.../\alpha_N$, for a laminate having N layers with layers 1 and N being the inner and the outer layers, respectively, implies that fibers in the kth layer are oriented at angle α_k measured counter-clockwise from the x-axis. Unless stated otherwise, each layer of a laminated shell is assumed to be of equal thickness. In Table 2, we have listed for the shell with all edges either clamped or simply supported, values of the nondimensional deflection, $\bar{w}\,(0.5a, 0.5b, 0)$, at the centroid of the mid-surface and the axial stress, $\bar{\sigma}_{xx}\,(0.5a, 0.5b, 0.5h)$, at the centroid of the top surface for six uniform n × m FE meshes with n and m equaling the number of elements along the x- and the y-axes, respectively. Unless mentioned otherwise, the displacement and the stresses are nondimensionalized as: $\bar{w} = w\,(h^3/b^4)E_2/q_0$ and $\bar{\boldsymbol{\sigma}} = \boldsymbol{\sigma}/q_0$. We note that numbers in the column "Diff." denote the change in the value from that obtained with the immediate previous FE mesh.

Results reported in Table 2 imply that with the mesh refinement the deflection converges faster than the axial stress and the convergence rate does not depend much upon the BCs. For simply supported edges the axial stress at the point $(0.5a, 0.5b, 0.5h)$ is nearly three times that for the clamped edges, and the deflection at the point $(0.5a, 0.5b, 0)$ for simply supported edges is five times that for the fixed edges. For both problems the 23×23 FE

Table 2. Convergence of solutions for a 0°/90°/0° laminated spherical shell ($a = b$, $R/a = 2$, $a/h = 10$).

	Clamped edges				Simply supported edges			
Mesh	$\bar{w} \times 10^3\ (0.5a, 0.5b, 0)$	%Diff.	$\bar{\sigma}_{xx}\ (0.5a, 0.5b, 0.5h)$	%Diff.	$\bar{w} \times 10^3\ (0.5a, 0.5b, 0)$	%Diff.	$\bar{\sigma}_{xx}\ (0.5a, 0.5b, 0.5h)$	%Diff.
15 × 15	1.829	—	25.081	—	9.178	—	72.788	—
17 × 17	1.829	0.0000	25.079	− 0.008	9.178	0.000	72.768	− 0.027
19 × 19	1.829	0.0000	25.077	− 0.008	9.178	0.000	72.753	− 0.021
21 × 21	1.829	0.0000	25.075	− 0.008	9.178	0.000	72.743	− 0.014
23 × 23	1.829	0.0000	25.074	− 0.004	9.178	0.000	72.735	− 0.011
25 × 25	1.829	0.0000	25.074	0.000	9.178	0.000	72.729	− 0.008

Table 3. Nondimensional deflection, $\bar{w}$ (0.5a, 0.5b, 0.5h) x 10^3, at the centroid of the outer-surface of the 0°/90° spherical shell.

	a/h = 100			a/h = 10		
R/a	3D LET [45]	TSNDT	%Diff.	3D LET [45]	TSNDT	%Diff.
1	0.0725	0.0726	− 0.14	6.6628	6.8453	− 2.74
2	0.2869	0.2870	− 0.03	13.2075	13.3982	− 1.44
3	0.6461	0.6465	− 0.06	16.1084	16.1938	− 0.53
4	1.1440	1.1447	− 0.06	17.4280	17.4427	− 0.08
5	1.7569	1.7580	− 0.06	18.1020	18.0743	− 0.15

mesh gives converged values of the two quantities. Unless stated otherwise, we use the 25 × 25 uniform FE mesh corresponding to 23,712 DoF.

3.2. *Comparison of TSNDT results with those from the 3D LET*

For different values of the length/thickness and (radius of curvature)/length ratios of the laminated doubly curved shell, we compare the TSNDT predictions with those from the 3D LET. Values of material parameters are listed in Section 3.1.

3.2.1. *Spherical shell*

We study deformations of a simply supported 0°/90° cross-ply laminated spherical shell with a uniform normal tensile traction, q_0, applied only on the outer surface. In Table 3, we have compared nondimensional deflection, $\bar{w}$ (0.5a, 0.5b, 0.5h), at the centroid of the top surface of the shell for $a = b$, a/h = 100 and 10, and different values of R/a found using the TSNDT with that given by the analytical 3D LET solution of Fan and Zhang [45]. There is at most 2.74% difference between the two sets of results for R/a = 1 and a/h = 10, and this difference decreases with an increase in R/a. The shell deflection increases with an increase in the ratio R/a.

3.2.2. *Cylindrical shell*

For simply supported [0°/90°/0°/ …] laminated cylindrical shells ($1/R_{2m} = 0$) subjected only on the outer surface to the sinusoidal distributed normal tensile traction:

$$q(x, y) = q_0 \sin(\pi x/a) \sin(\pi y/b), \tag{11}$$

we have compared in Table 4 values of the nondimensional deflection at the centroid of their mid-surfaces with $R_{1m}/a = 4$, $b/a = 3$, and a/h = 10 and 50 computed with the two theories. The two sets of results are in excellent agreement with each other

Table 4. Nondimensional deflection, $\bar{w}$ (0.5a, 0.5b, 0) x 10^2, at the centroid of mid-surface of a laminated cylindrical shell of N layers with $R_{1m}/a = 4$ and $b/a = 3$.

	N	2	3	4	5	10
a/h = 50	3-D LET [46]	2.139	0.5129	1.043	0.6059	0.9113
	TSNDT	2.132	0.5169	1.050	0.6101	0.9189
	%Diff.	0.33	− 0.78	− 0.67	− 0.69	− 0.83
a/h = 10	3-D LET [46]	2.783	0.9396	1.609	1.020	1.381
	TSNDT	2.787	0.8981	1.501	0.9524	1.314
	%Diff.	− 0.14	4.42	6.71	6.63	4.85

Table 5. Nondimensional stresses in the 90°/0° doubly curved shell with $a = b$, a/h = 10, $R_{1m}/a = 5$, and $R_{2m}/R_{1m} = 2$.

	z/h	3-D LET [47]	TSNDT	%Diff.
$\bar{\sigma}_{xx}$(0.5a, 0.5b, z)	0.5	72.5015	72.2213	0.39
	0+	− 55.7425	− 54.2168	2.74
	0−	− 1.5182	− 1.4397	5.17
	−0.5	− 8.2074	− 8.3104	− 1.25
$\bar{\sigma}_{yy}$(0.5a, 0.5b, z)	0.5	8.8503	8.8137	0.41
	0+	2.0775	2.0171	2.91
	0−	62.9176	62.4791	0.70
	−0.5	− 69.0028	− 69.0674	− 0.09
$\bar{\sigma}_{xz}$(0, 0.5b, z)	0.25	3.2347	3.1925	1.30
	0	1.3965	1.3937	0.20
	−0.25	0.9362	0.9414	− 0.56
$\bar{\sigma}_{yz}$(0.5a, 0, z)	0.25	0.727	0.7050	3.03
	0	0.9964	0.9680	2.85
	−0.25	3.1326	3.1665	− 1.08
$\bar{w}$ (0.5a, 0.5b, z)	0.5	11.9190	11.8748	0.37
	0	11.9581	11.9150	0.36
	−0.5	11.8910	11.8468	0.37

for thin shells. However, for thick shells, they differ at most by 6.71%.

3.2.3. *Doubly curved shells with different radii of curvature*

We now consider a simply supported 90°/0° cross-ply laminated doubly curved shell with $a = b$, a/h = 10, $R_{1m}/a = 5$, h = 10 mm, $R_{2m}/R_{1m} = 2$, and subjected only on the outer surface to sinusoidal distributed tensile traction given by Eq. (11). We have listed in Table 5 the nondimensional deflection and stresses at various locations through the shell thickness obtained by the two theories. For the TSNDT, the transverse stresses are computed using the SRS. The two sets of results differ by at most 5% implying that for this problem also the TSNDT with the SRS gives through-the-thickness stresses close to those obtained from the 3D LET [47].

3.3. *Clamped isotropic shell subjected to uniform normal traction on the outer surface*

3.3.1. *Comparison with the 3D LET solution*

3.3.1.1. *Spherical shell.* We study deformations of a clamped spherical shell made of an isotropic material with h = 10 mm, a/h = 10, $a = b$, R/a = 5, E = 210 GPa, $\nu = 0.3$, and a uniformly distributed tensile normal traction, q_0 = 10 MPa, applied only on the outer surface. In Figure 2, we have plotted the displacement, w (x, $b/2$, 0), of points on the mid-surface of the shell along the line $y = b/2$ obtained by using the TSNDT and the 3D LET solution computed with the FEM; the inset in the figure is a schematic of the problem studied. Results from the two theories agree well with each other having at most 0.3% difference between them. Stresses σ_{xx}(0.5a, 0.5b, 0.5h) and σ_{xz}(0.055a, 0.5b, 0) in the 3D LET solutions with uniform 100 × 100 × 10 and 80 × 80 × 10 meshes differed by only 0.07 and 0.6%, respectively.

In Figure 3a, we have exhibited through-the-thickness distributions of the axial stress, σ_{xx}, and the transverse normal stress, σ_{zz}, along the transverse normal passing through the centroid of the mid-surface. The axial stresses computed from the two theories differ by 0.82 and 0.42% at z = h/2 and –h/2, respectively. Because of the shell curvature, magnitudes of the axial

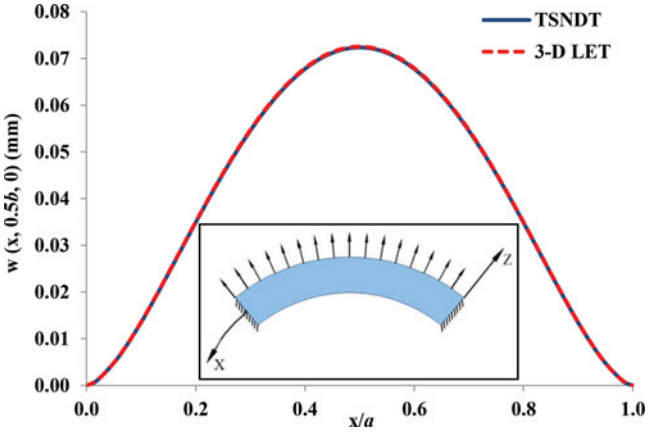

Figure 2. For a clamped spherical shell made of an isotropic material and subjected to a uniform normal tensile traction on the outer surface, variation of the z-displacement along the curvilinear line $y = b/2$ on the shell mid-surface.

tensile and the axial compressive stresses at corresponding points on the outer and the inner surfaces of the shell are different. The TSNDT transverse normal stress obtained directly from the constitutive relation does not exhibit the "boundary layer phenomenon" near major surfaces as predicted by the 3D LET and differs from the applied normal traction at the outer surface by 20%. However, this error is reduced to 2.7% and the boundary layer effect is captured when σ_{zz} is computed using the SRS. In Figure 3b, we have depicted through-the-thickness variations of the transverse shear stress, σ_{xz}, along the transverse

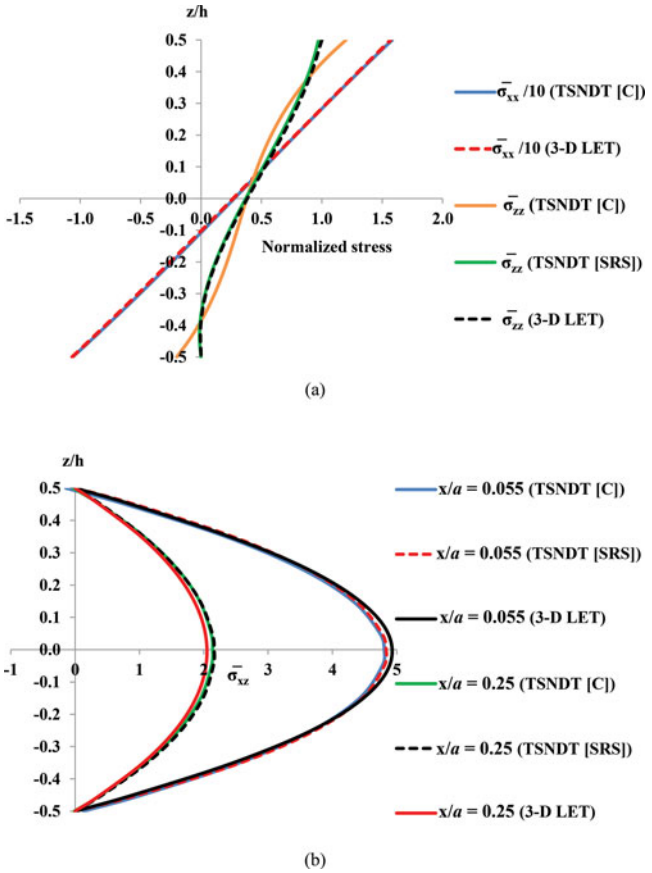

Figure 3. For a clamped spherical shell made of an isotropic material and loaded with a uniform normal tensile traction q_0 on the outer surface, through-the-thickness distributions of (a) $\bar{\sigma}_{xx}$ (0.5a, 0.5b, z) and $\bar{\sigma}_{zz}$ (0.5a, 0.5b, z), and (b) $\bar{\sigma}_{xz}$ at points (0.055a, 0.5b, z) and (0.25a, 0.5b, z). The stresses are normalized by q_0.

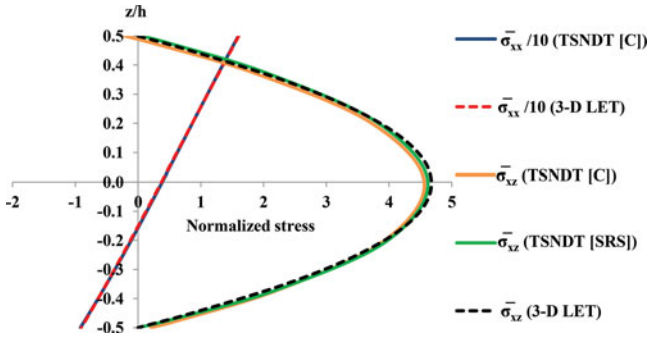

Figure 4. For a clamped doubly curved shell made of an isotropic material and subjected to a uniform normal tensile traction q_0 on the outer surface, through-the-thickness distributions of $\bar{\sigma}_{xx}$ (0.5a, 0.5b, z) and $\bar{\sigma}_{xz}$ (0.055a, 0.5b, z). The stresses are normalized by q_0.

normal near and away from the edge x = 0, passing through the points (0.055a, 0.5b, 0) and (0.25a, 0.5b, 0), respectively. It is evident that for both cases the TSNDT SRS stresses differ from the 3D LET stresses by at most 2.8% at z = 0. The transverse shear stress at the point (0.055a, 0.5b, 0) near the edge equals about 2.5 times that at the interior point (0.25a, 0.5b, 0). We note that the zero tangential traction boundary conditions at points (0.055a, 0.5b, ±h/2) near the clamped edge x = 0 are well satisfied when σ_{xz} is computed with the TSNDT and the SRS. However, these boundary conditions are well satisfied at points (0.25a, 0.5b, ±h/2) away from the edge x = 0 whether or not the SRS is used.

3.3.1.2. ***Doubly curved shell with two different radii of curvature.*** In Figure 4, we have portrayed through-the-thickness distributions of σ_{xx} and σ_{xz} along the transverse normal passing through points (0.5a, 0.5b, 0) and (0.055a, 0.5b, 0), respectively, for the problem studied in Subsection 3.3.1.1 but now with $R_1 = 3a$ and $R_2 = 2R_1$. The distributions of σ_{xx} obtained from the TSNDT and the 3D LET agree well with each other having the maximum difference of 1.5% at z = –h/2. However, at points (0.055a, 0.5b, ±h/2) near the edges on the two major surfaces of the shell, the traction boundary condition is well satisfied only if σ_{xz} is computed using the SRS. The maximum difference between the two values of σ_{xz} at points (0.055a, 0.5b, z) obtained using the SRS and the 3D LET is 1.37%.

3.3.1.3. ***Cylindrical shell.*** We now study deformations of a cylindrical clamped shell ($1/R_{m2} = 0$) composed of an isotropic material having h = 10 mm, $b/a = 2$, a/h = 10, and $R_{m1}/a = 1$, E = 210 GPa, $\nu = 0.3$, and subjected to a compressive vertical traction (i.e., parallel to the Cartesian X_3-axis) of magnitude $q_0 = 10$ MPa on the outer surface only. Thus, in the curvilinear (xyz) coordinate system this corresponds to combined normal (along the z-axis) and tangential (along the x-axis) nonuniform surface tractions. We have depicted in Figure 5 the z- and the x-displacements along the line y = b/2 on the mid-surface of the shell computed using the TSNDT and the 3D LET; the inset shows a schematic of the problem studied. It should be clear that the two sets of results agree well with each other having the maximum difference of 0.15% in w at x/a = 0.5 and 1.67% in u at x/a = 0.21 and 0.79.

We have portrayed in Figure 6a through-the-thickness distributions of the in-plane axial stresses (σ_{xx}, σ_{yy}) and in Figure 6b

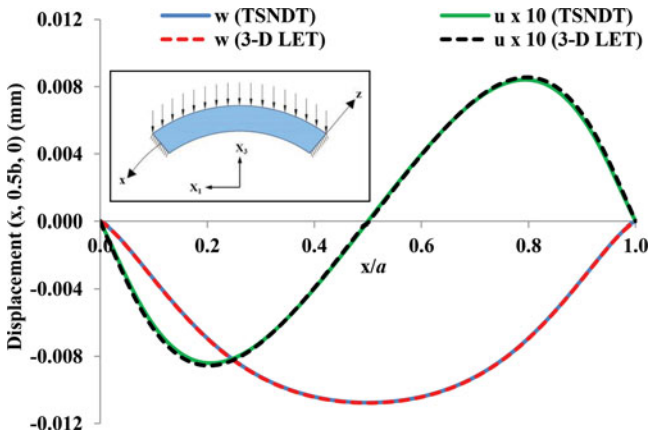

Figure 5. For a clamped cylindrical shell made of an isotropic material and subjected to a compressive load along the X_3-direction on the outer surface only, x- and z-displacements along the line $y = b/2$ on the mid-surface of the shell.

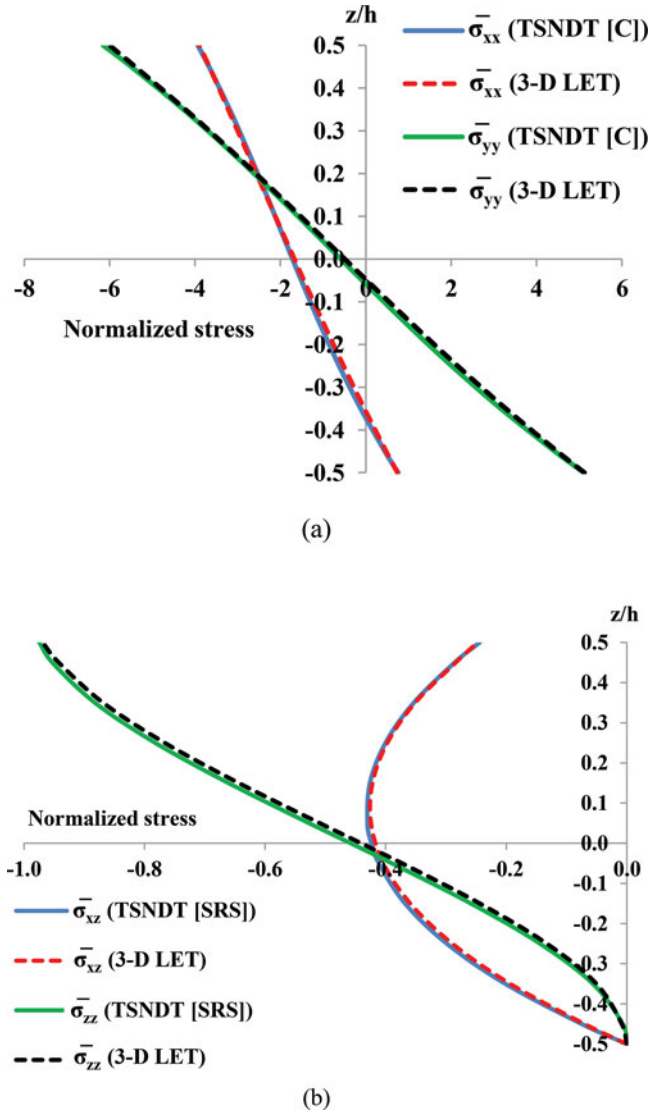

Figure 6. For a clamped cylindrical shell made of an isotropic material and subjected to a compressive load along the X_3-direction on the outer surface only, through-the-thickness distributions of (a) σ_{xx} and σ_{yy} at (0.5a, 0.5b, z) and (b) σ_{xz} and σ_{zz} at (0.25a, 0.5b, z). The stresses are normalized by q_0.

the transverse stresses (σ_{xz}, σ_{zz}) along the transverse normal passing through points (0.5a, 0.5b, 0) and (0.25a, 0.5b, 0), respectively. The differences in the magnitude of σ_{xx} at the centroid of the outer and the inner surfaces computed from the TSNDT and the 3D LET are 1.86 and 0.81%, respectively, and the corresponding differences for σ_{yy} are 0.25 and 2.52%. The transverse stresses computed using the TSNDT and the SRS satisfy the traction boundary conditions with only 0.57 and 1.3% error in the normal and the tangential traction at the point (0.25a, 0.5b, 0.5h) on the outer surface.

3.3.2. *Effect of shell's curvature on stress distributions*

In Figures 7a and 7b, we have depicted through-the-thickness distributions of σ_{xx} along the transverse normal passing through the centroid of the mid-surface and σ_{xz} computed using the SRS along points (0.055a, 0.5b, z) for clamped spherical shells studied in subsection 3.3.1. [illegible] R/a = 1, 2, 3, 10, 50. The inset in Figure 7a depicts curves of intersection of shell's mid-surfaces

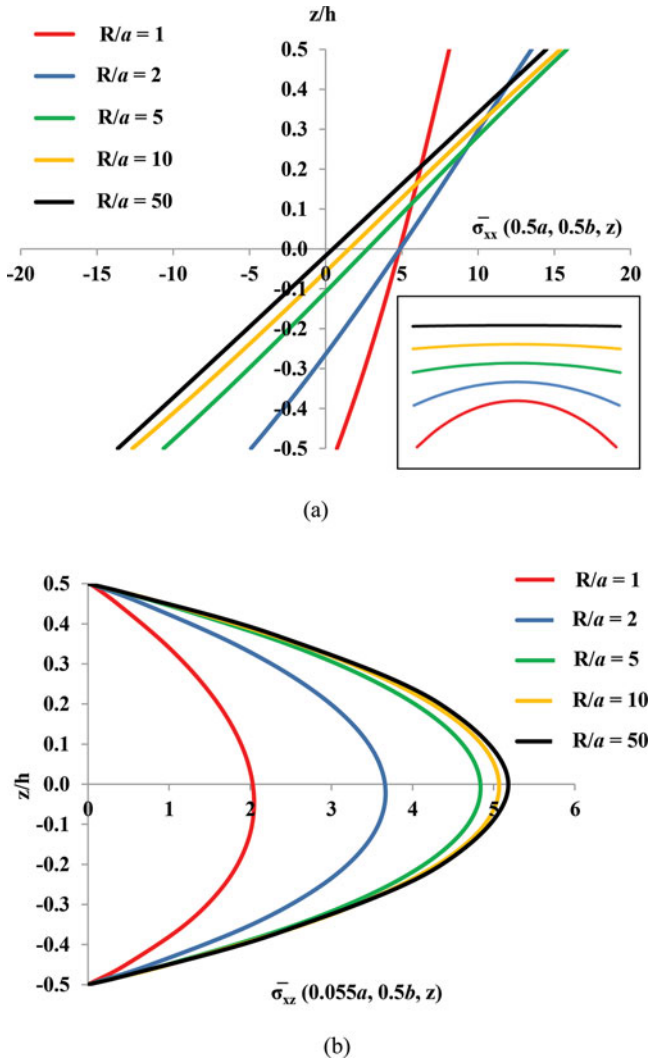

Figure 7. For a clamped spherical shell composed of an isotropic material and subjected to uniform normal tensile traction q_0 on the outer surface, through-the-thickness distributions of (a) $\bar{\sigma}_{xx}$ (0.5a, 0.5b, z) and (b) $\bar{\sigma}_{xz}$ at (0.055a, 0.5b, z) for different values of R/a. The stresses are normalized by q_0.

with a plane X_2 = constant. These results reveal that with an increase in the shell curvature, the plane of zero axial stress shifts towards the inner surface of the shell; thus, the portion of the shell in axial tension increases as compared to that in axial compression. For R/a = 1, the axial stress at all points on the transverse normal passing through the point (0.5a, 0.5b, 0) is tensile. The magnitude of the ratio of the axial stresses at the top and the bottom surfaces increases from 1.06 for R/a = 50 to 10.94 for R/a = 1. It is found that the magnitude of the transverse shear stress increases with a decrease in the shell curvature. However, the rate of increase in the magnitude of σ_{xz} slows down with an increase in the value of R/a. The magnitude of σ_{xz} at z = 0 for R/a = 50 is 2.54 and 1.02 times the corresponding value for R/a = 1 and 10, respectively.

3.3.3. *Effect of the loading on stress distributions*

For the problem studied in Subsection 3.3.1.3, we now consider four different applied loads, i.e., a uniform traction of magnitude 10 MPa on either the outer or the inner surface only pointing either radially (along the negative z-axis) or vertically (along the negative X_3-axis) downwards; these loads are denoted by q_r and q_v, respectively. For tractions along the X_3-axis, both normal and tangential tractions act on the shell surface. In Figures 8a and 8b, we have depicted through-the-thickness distributions of the axial stress, σ_{xx}, and the transverse shear stress, σ_{xz}, in the plane y = b/2 along the sections x = 0.5a and 0.25a, respectively. It is found that when the shell is subjected to the radial (vertical) load on the outer surface, the plane of zero axial stress intersects the transverse normal passing through the centroid of the mid-surface at z = –0.46h (–0.385h). Thus, a larger portion of the shell is in axial tension for the vertical traction as compared to that for the radial traction. The magnitudes of the maximum tensile and compressive axial stresses at the centroids of the inner and the outer surfaces for the vertical traction equal, respectively, 2.73 and 0.89 times that for the radial traction. Furthermore, due to the shell curvature, when the radial or the vertical traction is applied on the inner surface, the axial stress induced in the shell is different from that when the same traction is applied on the outer surface. When the inner surface is subjected to the radial traction, magnitudes of σ_{xx} at centroids of the inner and the outer surfaces, respectively, are 2.21 and 0.84 times that for the same traction applied on the outer surface, and the corresponding ratios for the vertical traction are 1.56 and 0.97.

Similarly, distributions of the transverse shear stress for the four applied tractions are different. When the traction is applied on the outer (inner) surface, the ratio of the magnitude of σ_{xz} at z = 0 for the vertical load to that for the radial load is 1.59 (0.86). Moreover, when the outer surface is subjected to the radial (vertical) load the magnitude of σ_{xz} at z = 0 is 1.06 (1.96) times that when the inner surface is subjected to the same load. Although not shown here for the sake of brevity, it is found that the axial stress changes only the sign with a negligible change in the magnitude when only direction of the applied load is changed for each of the four traction boundary conditions.

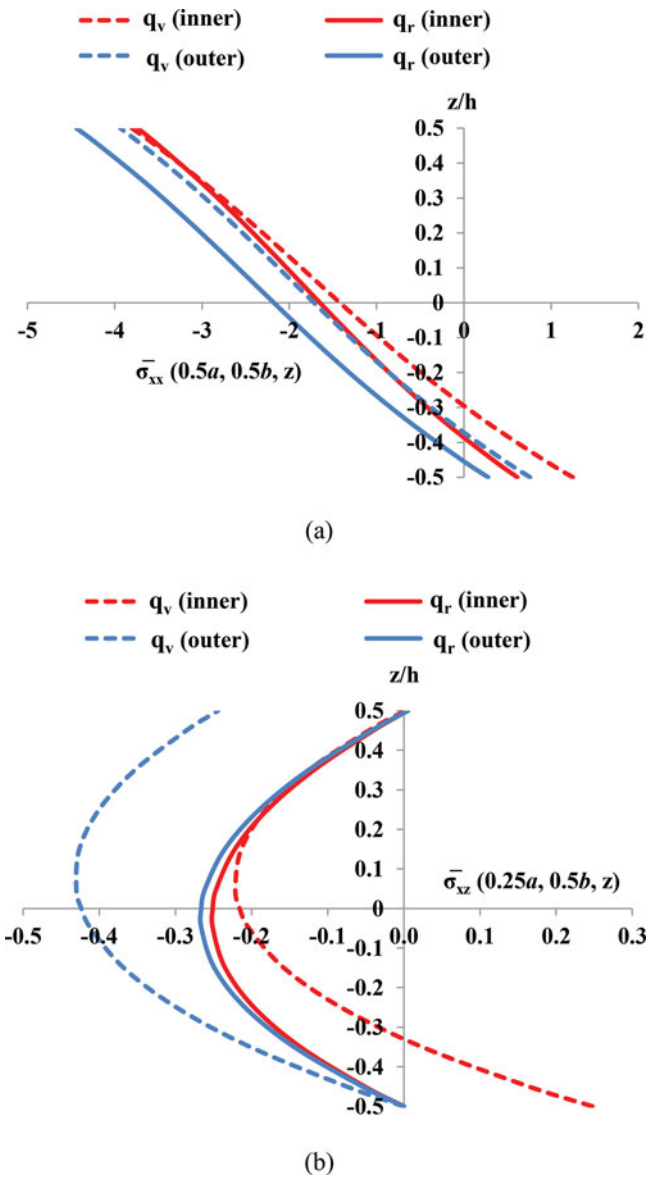

Figure 8. For a clamped cylindrical shell made of an isotropic material and subjected to four different loadings, through-the-thickness distributions of (a) σ_{xx} (0.5a, 0.5b, z) and (b) σ_{xz} (0.25a, 0.5b, z). Stresses are normalized by the magnitude of the applied traction.

3.3.4. *Effect of geometric parameters on the strain energy of deformation*

The total strain energy, W, of deformation is given by:

$$W = \sum_{j=1}^{6} W_j, \tag{12}$$

where

$$W_1 = \frac{1}{2}\sum_{k=1}^{N}\int_{\Omega^k} \sigma_{xx}^k \in_{xx}^k d\Omega^k, \quad W_2 = \frac{1}{2}\sum_{k=1}^{N}\int_{\Omega^k} \sigma_{yy}^k \in_{yy}^k d\Omega^k,$$

$$W_3 = \sum_{k=1}^{N}\int_{\Omega^k} \sigma_{xy}^k \in_{xy}^k d\Omega^k,$$

$$W_4 = \sum_{k=1}^{N} \int_{\Omega^k} \sigma_{xz}^k \ \epsilon_{xz}^k \ d\Omega^k, \quad W_5 = \sum_{k=1}^{N} \int_{\Omega^k} \sigma_{yz}^k \ \epsilon_{yz}^k \ d\Omega^k,$$

$$W_6 = \frac{1}{2} \sum_{k=1}^{N} \int_{\Omega^k} \sigma_{zz}^k \ \epsilon_{zz}^k \ d\Omega^k. \tag{12.1}$$

Alternatively, W can be written as the sum of strain energies of the in-plane (W_i), the transverse shear (W_s), and the transverse normal (W_n) deformations, i.e.,

$$W = W_i + W_s + W_n, \tag{13}$$

where $W_i = W_1 + W_2 + W_3$, $W_s = W_4 + W_5$, and $W_n = W_6$.

We substitute for u_i from Eq. (3) into Eq. (2) to write physical components of the infinitesimal strain tensor as:

$$\epsilon_{\alpha\beta} = (y_3)^b \ \epsilon_{\alpha\beta}^b, \tag{14}$$

where

$$\epsilon_{\alpha\beta}^b = \left(\frac{e_{\alpha\beta}^b}{2H_{(\beta)}} + \frac{e_{\beta\alpha}^b}{2H_{(\alpha)}} \right),$$

$$e_{11}^b = \frac{\partial u_{1b}}{\partial y_1} + \frac{u_{3b}}{R_1}, \ e_{12}^b = \frac{\partial u_{1b}}{\partial y_2}, \ e_{13}^b = D_{jb} u_{1j},$$

$$e_{21}^b = \frac{\partial u_{2b}}{\partial y_1}, \ e_{22}^b = \frac{\partial u_{2b}}{\partial y_2} + \frac{u_{3b}}{R_2}, \ e_{23}^b = D_{jb} u_{2j},$$

$$e_{31}^b = \frac{\partial u_{3b}}{\partial y_1} - \frac{u_{1b}}{R_1}, \ e_{32}^b = \frac{\partial u_{3b}}{\partial y_2} - \frac{u_{2b}}{R_2}, \ e_{33}^b = D_{jb} u_{3j},$$

$$D_{10} = 1, \ D_{21} = 2, \ D_{32} = 3, \ D_{ij} = 0 \ (i \neq j + 1). \tag{14.1}$$

In the above expressions, indices b, i, and j take values 0, 1, 2, and 3, and other indices take values 1, 2, and 3. The repeated index in the parentheses is not summed. We substitute for $\epsilon_{\alpha\beta}$ from Eq. (14) into Eq. (6) to obtain components of the Cauchy stress tensor as:

$$\sigma_{\alpha\beta} = (y_3)^b \ \sigma_{\alpha\beta}^b, \tag{15}$$

where

$$\sigma_{\alpha\beta}^b = C_{\alpha\beta mn} \ \epsilon_{mn}^b, \tag{15.1}$$

in which, indices α, β, m, and n take values 1, 2, and 3, and b takes values 0, 1, 2, and 3.

Thus, Eq. (12) representing the total strain energy of deformation can be written as:

$$W = W_{\text{stretch-in}} + W_{\text{bend-in}} + W_{\text{stretch-tr}} + W_{\text{bend-tr}} + W_{\text{couple}}, \tag{16}$$

where $W_{\text{stretch-in}}$ and $W_{\text{bend-in}}$ are strain energies of stretching and bending deformations, respectively, corresponding to the in-plane strains, $W_{\text{stretch-tr}}$ and $W_{\text{bend-tr}}$, are those corresponding to the transverse strains, and W_{couple} is the strain energy due to coupling between stretching and bending deformations; their expressions are given below:

$$W_{\text{stretch-in}} = \frac{1}{2} \sum_{k=1}^{N} \int_{\Omega^k} \left[(y_3)^m (y_3)^n (\sigma_{11}^m \ \epsilon_{11}^n + 2\sigma_{12}^m \ \epsilon_{12}^n + \sigma_{22}^m \ \epsilon_{22}^n) \right] d\Omega^k \ (m, \ n = 0, \ 2)$$

$$W_{\text{bend-in}} = \frac{1}{2} \sum_{k=1}^{N} \int_{\Omega^k} \left[(y_3)^m (y_3)^n (\sigma_{11}^m \ \epsilon_{11}^n + 2\sigma_{12}^m \ \epsilon_{12}^n + \sigma_{22}^m \ \epsilon_{22}^n) \right] d\Omega^k \ (m, \ n = 1, \ 3)$$

$$W_{\text{stretch-tr}} = \frac{1}{2} \sum_{k=1}^{N} \int_{\Omega^k} \left[(y_3)^m (y_3)^n (2\sigma_{13}^m \ \epsilon_{13}^n + 2\sigma_{23}^m \ \epsilon_{23}^n + \sigma_{33}^m \ \epsilon_{33}^n) \right] d\Omega^k \ (m, \ n = 1, \ 3)$$

$$W_{\text{bend-tr}} = \frac{1}{2} \sum_{k=1}^{N} \int_{\Omega^k} \left[(y_3)^m (y_3)^n (2\sigma_{13}^m \ \epsilon_{13}^n + 2\sigma_{23}^m \ \epsilon_{23}^n + \sigma_{33}^m \ \epsilon_{33}^n) \right] d\Omega^k \ (m, \ n = 0, \ 2)$$

$$W_{\text{couple}} = \frac{1}{2} \sum_{k=1}^{N} \int_{\Omega^k} \left[(y_3)^p (y_3)^q \sigma_{ij}^p \ \epsilon_{ij}^q + (y_3)^r (y_3)^s \sigma_{ij}^r \ \epsilon_{ij}^s \right] d\Omega^k \ (i, \ j = 1, \ 2, \ 3; \ p, \ s = 0, \ 2; \ q, \ r = 1, \ 3) \tag{16.1}$$

We note that for a plate W_{couple} equals zero.

We consider a clamped doubly curved shell with $a = b =$ 10 cm, made of an isotropic material with E = 210 GPa, $\nu =$ 0.3, and subjected to a uniform normal tensile traction, $q_0 =$ 10 MPa, on its outer surface only, and investigate effects of the aspect ratio, a/h, the normalized radius of curvature, R_{1m}/a, and the curvature ratio, R_{2m}/R_{1m}, of the shell on strain energies of different deformations. For static elastic deformations of the shell, the total strain energy of deformation, W, equals the work done by external forces, W_e. It should be clear from values listed in Table 6 that W and W_e differ by at most 3.14%. This further verifies the accuracy of the computed results.

Table 6. Strain energy, W, of deformation and work done, W_e, by the external force for shells with $a = b = 10$ cm.

a/h	R_{1m}/a	R_{2m}/R_{1m}	W_e (mJ)	W (mJ)	%Error
10	1	5	734	730	0.54
		2	651	648	0.46
		1	494	494	0.00
5	1	5	232	238	−2.59
		2	223	230	−3.14
		1	198	204	−3.03

3.3.4.1. *Strain energies of in-plane and transverse deformations.*

3.3.4.1.1. *Effect of aspect ratio.* We first assume $R_{1m} = R_{2m} = R$ and illustrate in Figure 9a the effect of the aspect ratio, a/h, for three values of the radius of curvature, $R/a = 1$, 10 and ∞ (plate), on strain energies of in-plane and transverse deformations. Unless mentioned otherwise, strain energies of different deformation modes plotted in the following several figures are normalized with respect to the total strain energy of deformation, W, for each configuration of the shell. Values of W for shells with $R/a = 1$ and 10 and different aspect ratios listed in Table 7 indicate that for the spherical shell with given a and R, the total strain energy of deformation increases with an increase in the aspect ratio. It is clear from plots of Figure 9a that, for a given curvature, the strain energy of in-plane deformations increases

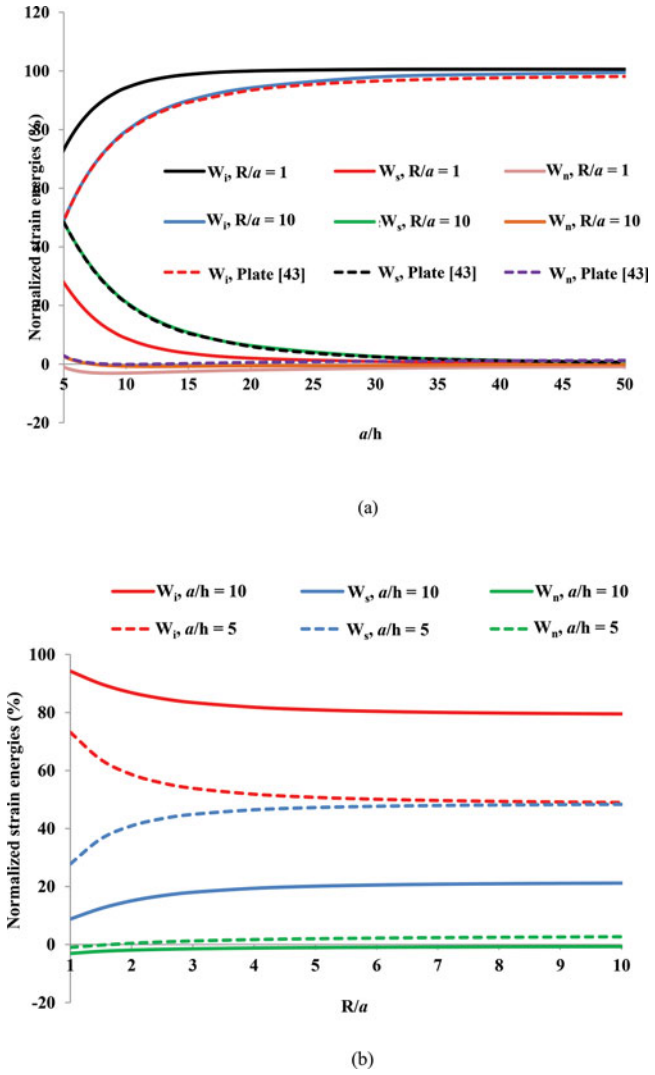

Figure 9. Variation with (a) the aspect ratio, *a*/h, and (b) the normalized radius of curvature, R/*a*, of normalized values of strain energies of deformation due to in-plane, transverse shear, and transverse normal deformations for a monolithic clamped spherical shell made of an isotropic material subjected to a uniform normal tensile traction on the outer surface. Plotted energies are normalized with respect to W (listed in Tables 7 and 8) for each configuration of the shell.

and that of transverse shear and transverse normal deformations decreases with an increase in the aspect ratio. We note that the strain energies, W_4, W_5, and W_6, of transverse deformations have been computed with stresses found using the SRS and the corresponding strains by pre-multiplying the stress tensor with the compliance matrix. For R/a = 1 and a/h = 5, the contributions to the normalized total strain energy of deformation from in-plane and transverse shear deformations are 73.2 and 23.8%, respectively. For a/h > 20, strain energies due to transverse shear deformations become negligible and those due to in-plane deformations dominate. This agrees with results of [51] in that for a/h > 20 predictions from shear deformation theories converge to those from the classical theory, which neglects transverse shear deformations. The strain energies of the shell with R/a = 10 nearly equal those for the plate. We note that results for the plate included in Figure 9a are from our earlier work [43].

Table 8. Total strain energy of deformation, W (mJ), for clamped spherical shells with different values of the radius of curvature; $a = b = 10$ cm.

R/a	1	2	3	4	5	6	7	8	9	10
a/h = 5	204	258	268	270	271	270	270	270	269	269
a/h = 10	494	905	1074	1148	1184	1204	1216	1224	1229	1233

3.3.4.1.2. *Effect of the shell curvature.* We have demonstrated in Figure 9b for the clamped spherical shell the effect of the normalized radius of curvature, R/a, for two values of the aspect ratio, a/h = 5 and 10, on two components of the strain energy of deformation. With an increase in R/a (i.e., a decrease in the curvature), the strain energy of in-plane deformations decreases and that of transverse shear and transverse normal deformations increases. However, the rate of decrease and increase in W_i and W_s, respectively, slows down with an increase in the magnitude of R/a. For example, for the shell with a/h = 10 the contribution to the normalized total strain energy of deformation from in-plane deformations decreases from 94.3% for R/a = 1 to 80.7 and 79.5% for R/a = 5 and 10, respectively. For all shell configurations studied, the strain energy due to transverse normal deformations is found to be less than 3% of the total strain energy. In Table 8, we have reported for spherical shells with a/h = 5 and 10 values of W for different R/a ratios.

3.3.4.1.3. *Effect of the curvature ratio.* We now consider the shell with $R_{1m}/a = 1$, and different values of $R_{2m} > R_{1m}$. In Table 9, we have listed values of W for these shells. For a thick shell with a/h = 5, values of R_2/R_1 between 2 and 5 have a negligible effect on W. However, for a shell with a/h = 10, the value of W increases from 648 to 730 mJ with an increase in R_2/R_1 from 2 to 5. In Figure 10, we have portrayed the effect of the curvature ratio, R_{2m}/R_{1m}, on strain energies of the in-plane and the transverse deformations for a/h = 5 and 10. It is found that the strain energy of the in-plane deformations decreases and that of the transverse shear and the transverse normal deformations increases with an increase in the curvature ratio. The normalized value of W decreases by 4.8 and 12.6% in going from R_{2m}/R_{1m} = 1 to 5 for a/h = 10 and 5, respectively, while the corresponding increase in the normalized values of W_i are 40.4 and 28.7%. For a/h = 5 and R_{2m}/R_{1m} = 5, the strain energy of transverse shear deformations accounts for 35.8% of the total strain energy of deformation.

Table 7. Total strain energy of deformation, W (mJ), for spherical shells with different values of the aspect ratio; (a = b = 10 cm).

a/h	5	6	7	8	9	10	15	20	25	30	40	50
R/a = 1	204	253	308	367	429	494	837	1190	1547	1909	2643	3388
R/a = 10	269	382	530	718	951	1233	3555	7778	14318	23668	49917	86984

Table 9. Total strain energy of deformation, W (mJ), for doubly curved shells with different ratios of the radii of curvature; (a = b = 10 cm).

R_2/R_1	2	3	4	5
a/h = 5	230	235	237	238
a/h = 10	648	696	718	730

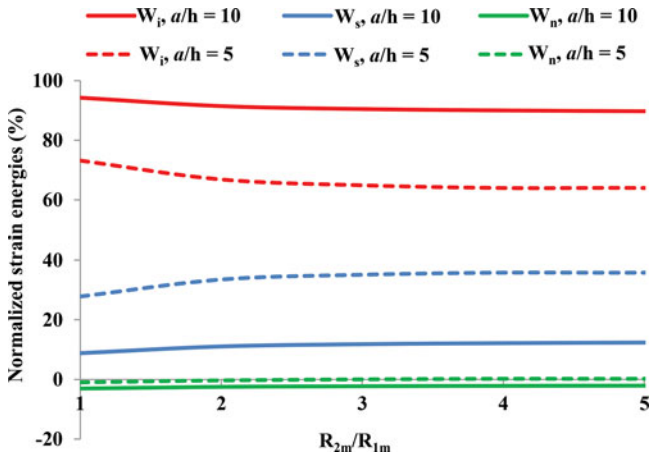

Figure 10. Variation with the curvature ratio, R_{2m}/R_{1m}, of the normalized strain energies of deformation due to in-plane, transverse shear, and transverse normal deformations for a monolithic clamped doubly curved shell made of an isotropic material subjected to a uniform normal tensile traction on the outer surface. Plotted energies are normalized with respect to W (listed in Table 9) for each configuration of the shell.

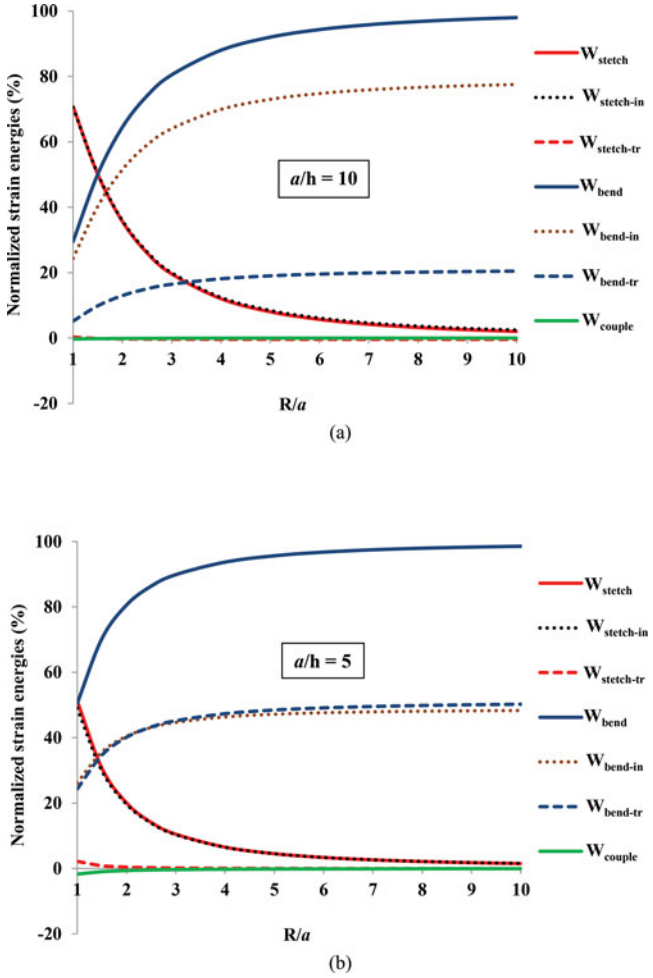

Figure 11. Variation with the normalized radius of curvature, R/*a*, of the normalized values of strain energies of deformation due to stretching and bending deformations for a monolithic clamped spherical shell made of an isotropic material with (a) *a*/h = 10, (b) *a*/h = 5, and subjected to a uniform normal tensile traction on the outer surface. Plotted energies are normalized with respect to W (listed in Table 8) for each configuration of the shell.

3.3.4.2. *Strain energies of stretching and bending deformations.*

3.3.4.2.1. *Effect of the shell curvature.* For a spherical shell with *a*/h = 10 and 5 we have plotted in Figures 11a and 11b, respectively, the effect of the ratio R/*a* on strain energies of stretching and bending deformations. We note that $W_{stretch} = W_{stretch\text{-}in} + W_{stretch\text{-}tr}$ and $W_{bend} = W_{bend\text{-}in} + W_{bend\text{-}tr}$. It is found that for a given aspect ratio, the strain energy of bending (stretching) deformations increases (decreases) with an increase in R/*a*. However, the rate of increase (decrease) in W_{bend} ($W_{stretch}$) slows down with an increase in R/*a*. For example, for the shell with *a*/h = 5, the normalized value of W_{bend} ($W_{stretch}$) is 50.5% (51.2%) when R/*a* = 1 and it increases (decreases) to 95.6% (4.5%) and 98.6% (1.5%) when R/*a* = 5 and 10, respectively. For the shell with *a*/h = 10, contributions from W_{bend} and $W_{stretch}$ to the total strain energy of deformations are 29.5 and 70.8%, respectively, for R/*a* = 1 and the corresponding values for R/*a* = 10 are 98 and 2%.

It is observed that for the shell with *a*/h = 10, the contribution to W_{bend} from in-plane deformations is higher than that from transverse deformations. However, for the thick shell (*a*/h = 5), in-plane and transverse deformations contribute about equally to the total strain energy of bending deformations. For example, when R/*a* = 10 bending deformations due to in-plane and transverse strains account for 77.5 and 20.5%, respectively, of the total strain energy of deformation for *a*/h = 10 and the corresponding values for *a*/h = 5 are 48.3 and 50.2%.

The strain energy of stretching deformations due to transverse strains, $W_{stretch\text{-}tr}$, is at most 2.2% and the magnitude of W_{couple} representing the interaction between stretching and bending deformations is at most 1.7%, which is negligible as compared to other components of the strain energy; these maximum values correspond to the shell with R/*a* = 1 and *a*/h = 5.

3.3.4.2.2. *Effect of the aspect ratio.* We have elucidated in Figures 12a and 12b the effect of the aspect ratio, *a*/h, on strain energies of stretching and bending deformations for a spherical shell with R/*a* = 10 and 1, respectively. It is clear that the strain energy of stretching (bending) deformations increases (decreases) with an increase in the aspect ratio. For the shell with R/*a* = 10, (W_{bend}, $W_{stretch}$) = (98.5%, 1.5%) of W when *a*/h = 5 and equals (69.6%, 30.4%) of W when *a*/h = 50. Note that the effect of transverse deformations has been included in these two energies. For the deep shell (R/*a* = 1), the rate of increase (decrease) of $W_{stretch}$ (W_{bend}) slows down with an increase in the magnitude of *a*/h. For example, $W_{stretch}$ increases from 0.512W for *a*/h = 5 to 0.9W and 0.945W for *a*/h = 25 and 50, respectively.

For an isotropic cylindrical shell (R_2 = R, $1/R_1 = 0$), Calladine [48] computed the ratio of the stretching and the bending stiffnesses as $\xi = \frac{12}{\pi^4}\frac{a^4(1-\nu^2)}{R^2h^2}[1 + (a/b)^2]^{-4}$. Thus, for a shell with $\nu = 0.3$, R/*a* = 1, and *a* = *b*, the stretching stiffness will exceed 10 times the bending stiffness when *a*/h > 37. The corresponding aspect ratio for the spherical shell for the strain energy of stretching deformations to exceed that of bending deformations is found to be about 30 from the plots of Figure 12b. Furthermore, the expression for ξ suggests that for fixed values of *a* and *b*, the stretching stiffness dominates over the bending stiffness as either the aspect ratio increases for a given curvature or the curvature increases for a given aspect ratio.

The strain energy of stretching deformations is mainly due to in-plane strains with negligible contribution from that due to

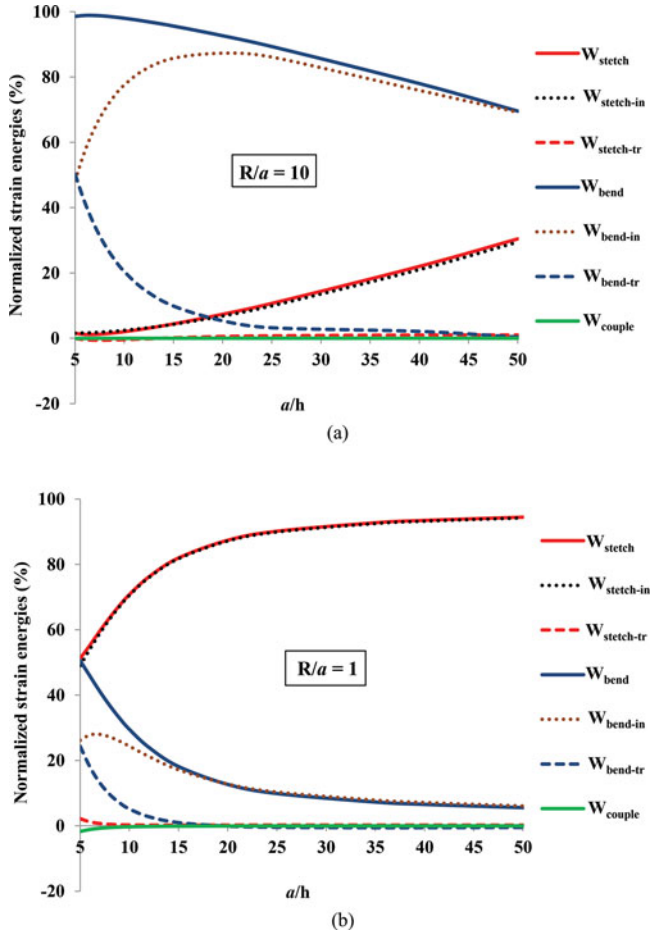

Figure 12. Variation with the aspect ratio, a/h, of the normalized values of strain energies of deformation due to stretching and bending deformations for a monolithic clamped spherical shell made of an isotropic material with (a) R/a = 10, (b) R/a = 1, and subjected to a uniform normal tensile traction on the outer surface. Plotted energies are normalized with respect to W (listed in Table 7) for each configuration of the shell.

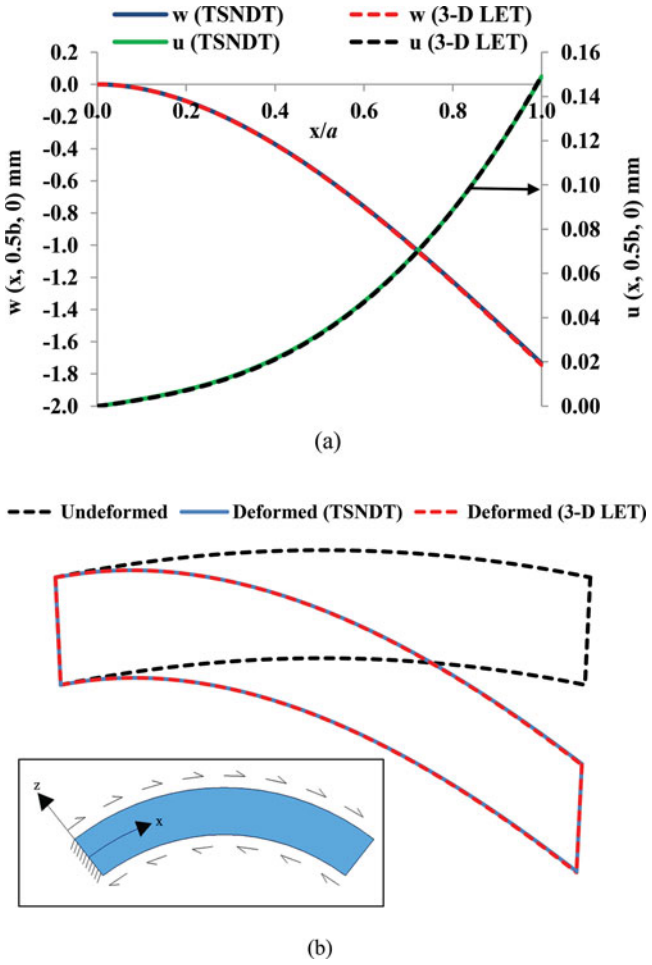

Figure 13. For a cantilever shell made of an isotropic material and subjected to equal and opposite uniform tangential tractions on the outer and the inner surfaces: (a) x- and z-components of displacement along the line y = b/2 on the mid-surface of the shell and (b) deformed shape of the cross-section y = b/2 with displacements magnified by a factor of 10.

transverse strains. The contribution to the strain energy of bending deformations from the transverse strains decreases monotonically with an increase in the aspect ratio. For example, $W_{bend\text{-}tr}/W$ for R/a = 10 and 1, respectively, equals 50.2 and 24.3% when a/h = 5 and decreases to 9.9 and 1% when a/h = 15. However, with an increase in the aspect ratio, the strain energy of bending deformations due to in-plane strains increases for a/h $\leq \beta$ and decreases for a/h $> \beta$, where β equals 25 and 7 for R/a = 10 and 1, respectively.

3.4. *Cantilever isotropic shell subjected to equal and opposite uniformly distributed tangential tractions on the outer and the inner surfaces*

These problems are motivated by the observation that during entry of a ship or a boat hull into water both tangential and normal tractions act on the hull/water interface. Similarly, surfaces of a fish moving in water are subjected to both normal and tangential tractions. For linear problems, the principle of superposition enables one to study separately problems for normal and tangential tractions.

3.4.1. *Comparison with the 3D LET solution*

We analyze deformations of a spherical shell clamped at the edge x = 0, with the remaining three edges traction free, having h = 10 mm, a/h = 10, a = b, R/a = 5, made of an isotropic material with E = 210 GPa, ν = 0.3, and equal and opposite uniform tangential tractions of magnitude q_0 = 10 MPa applied on the outer and the inner surfaces. We have depicted in Figure 13a the z- and the x-displacements along the line y = b/2 on the mid-surface of the shell with their scales on the left and the right vertical axes, respectively, and in Figure 13b the deformed shape of the cross section at y = b/2; the inset is the schematic of the problem studied. The results from the TSNDT and the 3D LET are in excellent agreement with each other having at most 0.5% difference between them for the two displacement components.

In Figures 14a and 14b, we have portrayed through-the-thickness distributions of the axial stress, σ_{xx}, and the transverse shear stress, σ_{xz}, along different transverse normal sections near and away from the edges x = 0 and x = a. The axial stress along the transverse normal passing through points (0.055a, 0.5b, 0), (0.5a, 0.5b, 0), and (0.945a, 0.5b, 0), respectively, computed using the TSNDT differs from the corresponding 3D LET solution at most by 3.1, 1.4, and 2.6%; these maximum differences

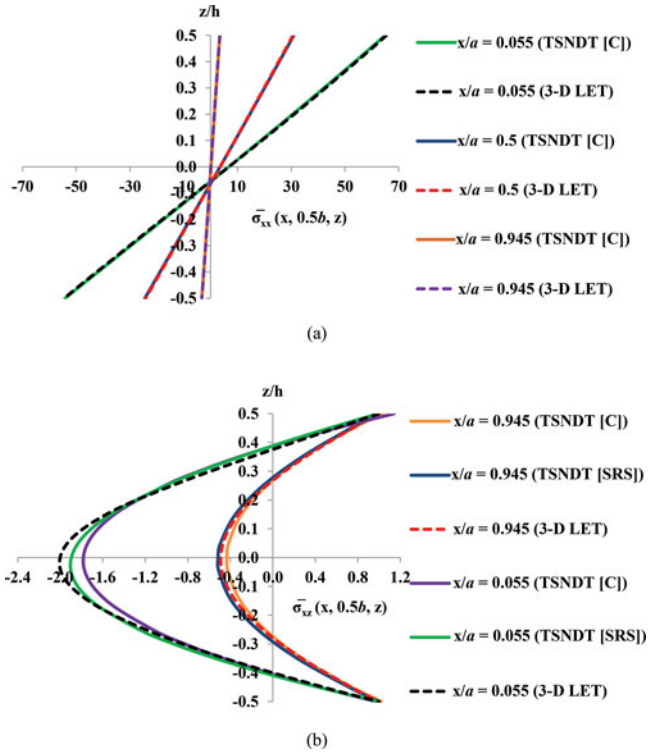

Figure 14. For a cantilever shell made of an isotropic material and subjected to equal and opposite uniform tangential tractions q_0 on the outer and the inner surfaces, through-the-thickness distributions of (a) σ_{xx}(x, 0.5b, z) for x/a = 0.055, 0.5, and 0.945, and σ_{xz}(x, 0.5b, z) for x/a = 0.055 and 0.945. The stresses are normalized by q_0.

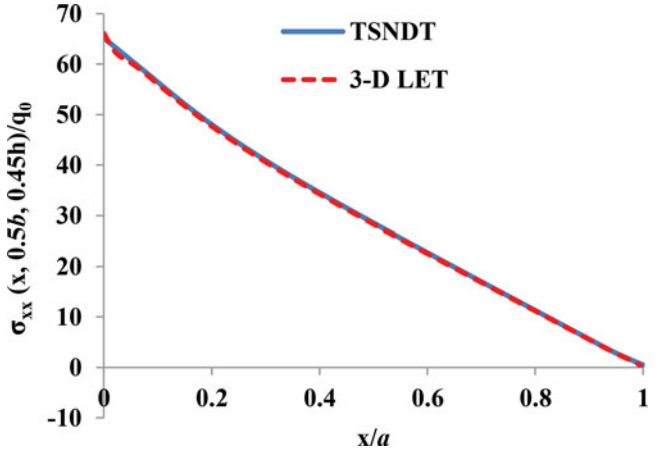

Figure 15. For a cantilever shell made of an isotropic material and subjected to equal and opposite uniform tangential tractions on the outer and the inner surfaces, variation of σ_{xx}(x, 0.5b, 0.45h) along the length in the x-direction of the shell.

occur at z/h = −0.15, −0.5, and 0.15, respectively. The magnitudes of σ_{xx} at corresponding points on the outer and the inner surfaces of the shell are different due to the curvature of the shell. Furthermore, the magnitude of the axial stress at points (x, b/2, h/2) located along the line at the intersection of the outer surface and the cross section y = b/2, for x = 0.055a is about 2 times and 19 times that for x = 0.5a and 0.945a, respectively. The transverse shear stress near the clamped edge obtained from the constitutive relation differs from the applied tangential traction at points (0.055a, 0.5b, –0.5h) and (0.055a, 0.5b, 0.5h) on the outer and the inner surfaces by 2.78 and 14.23%, respectively, and the corresponding differences near the traction free edge, x = a, at points (0.945a, 0.5b, –0.5h) and (0.945a, 0.5b, 0.5h) are 2.2 and 3.56%, respectively. However, these differences at (0.055a, 0.5b, 0.5h) and (0.945a, 0.5b, 0.5h) reduce to 0.69 and 0.5% when σ_{xz} is computed using the SRS. We note that at the inner surface of the shell σ_{xz} computed using the SRS exactly satisfies the tangential traction boundary condition, since the applied traction there is used as an initial condition during the integration of the equilibrium equations. The transverse shear stress computed directly from the constitutive relation differs from the corresponding 3D LET solution at most by 12.56 and 9.6% for x = 0.055a and 0.945a, respectively. However, these differences reduce to 8.04 and 7.9% when σ_{xz} is computed using the SRS. We have not checked if refining the FE mesh near the edges (i.e., using a graded FE mesh) will reduce these differences. The maximum value of σ_{xz} in the plane y = b/2 along the transverse normal section at x = 0.055a is about 3.75 times that for x = 0.945a.

In Figure 15, we have exhibited the variation of σ_{xx} along the length in the x-direction of the shell at y = b/2 and z = 0.45h computed using the TSNDT and the 3D LET. The two sets of results agree well with each other. At the clamped edge, the difference between values of the axial stress computed from the two theories is 1.44%; this difference reduces to 0.95% at x/a = 0.055 and 0.92% at x/a = 0.5. At the free edge, x = a, σ_{xx} accurately satisfies the zero traction boundary condition. The axial stress is maximum at a point located on the clamped edge, x = 0, and decreases with an increase in the distance of the point from the clamped edge.

3.4.2. *Effect of the curvature on stress distributions*

In Figures 16a and 16b, we have elucidated the effect of the curvature on through-the-thickness distributions of σ_{xx} and σ_{xz} along the transverse normal passing through the centroid of the mid-surface and the point (0.055a, 0.5b, 0) near the clamped edge x = 0, respectively. It is found that the magnitude of σ_{xx} increases, that of σ_{xz} decreases, and the plane of the zero axial stress shifts towards the mid-surface of the shell with an increase in the R/a ratio. However, the rate of increase and decrease in magnitudes of σ_{xx} and σ_{xz} slows down with an increase in the value of R/a. For example, the normalized magnitude of σ_{xx} at the point (0.5a, 0.5b, 0.5h) on the outer surface of the shell increases from 18.1 for R/a = 1 to 30.4 for R/a = 5 and to 30.6 for R/a = 10. The normalized magnitude of σ_{xz} at the point (0.5a, 0.5b, 0) on the mid-surface of the shell decreases from 6 for R/a = 1 to 1.9 for R/a = 5 and further to 1.6 for R/a = 10.

3.4.3. *Effect of geometric parameters on the strain energy of deformation*

We investigate the effect of the aspect ratio and the shell curvature on strain energies of different deformations for the problem studied in Subsection 3.4.1 with a = b = 10 cm.

3.4.3.1. *Strain energies of in-plane and transverse deformations.*

3.4.3.1.1. *Effect of the aspect ratio.* We have demonstrated in Figure 17a for a spherical shell the effect of the aspect ratio, a/h, for R/a = 1 and 10, on strain energies of in-plane and transverse

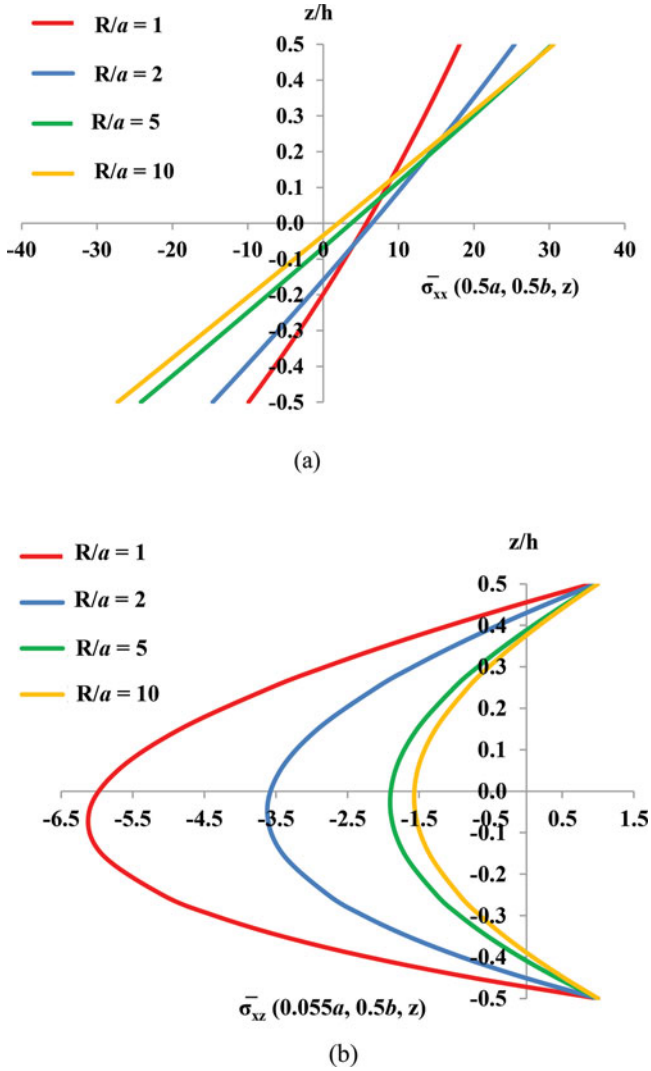

Figure 16. For a cantilever spherical shell made of an isotropic material and subjected to equal and opposite uniform tangential tractions on the outer and the inner surfaces, through-the-thickness distributions of (a) $\bar{\sigma}_{xx}$ (0.5a, 0.5b, z) and (b) $\bar{\sigma}_{xz}$ at (0.055a, 0.5b, z) for different values of R/a. The stresses are normalized by q_0.

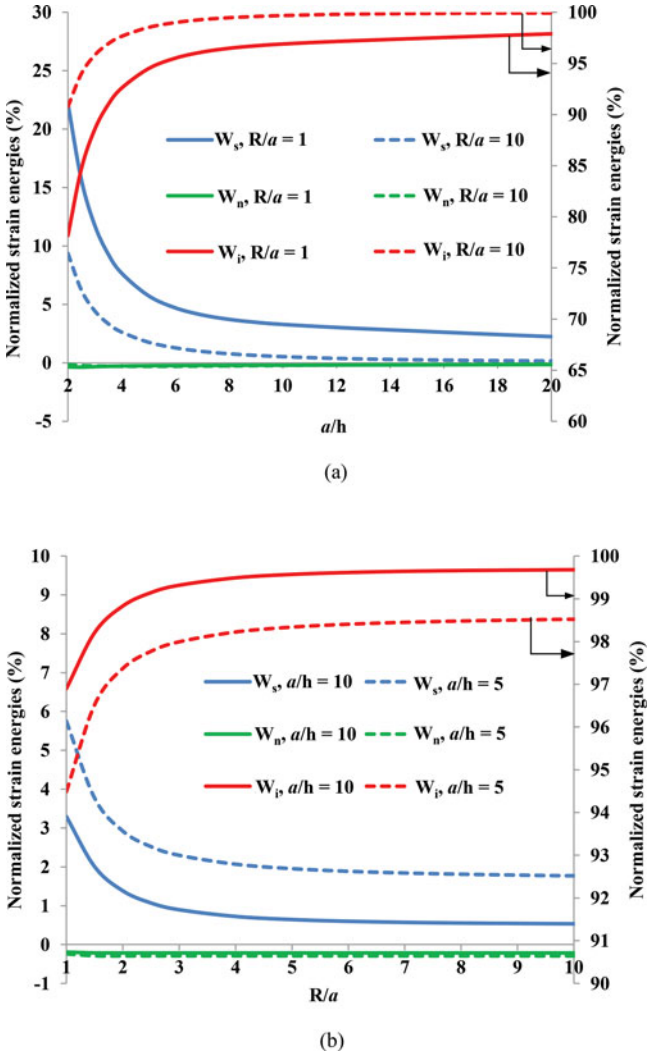

Figure 17. Variation with (a) the normalized radius of curvature, R/a, and (b) the aspect ratio, a/h, of normalized values of the strain energy due to in-plane, transverse shear, and transverse normal deformations for a monolithic cantilever spherical shell made of an isotropic material and subjected to equal and opposite uniform tangential tractions on the outer and the inner surfaces. Plotted energies are normalized with respect to W (Tables 10 and 11) for each configuration of the shell.

deformations with their scales given on the right and the left vertical axes, respectively. The results reveal that the strain energy of in-plane deformations increases and that of transverse shear and transverse normal deformations decreases with an increase in the aspect ratio of the shell. For R/a = 1, the in-plane and the transverse shear deformations contribute 78.2 and 22.2%, respectively, to the total strain energy of deformation when a/h = 2. The normalized strain energy of in-plane deformations increases to 94.5 and 99.7% when a/h = 5 and 10, respectively, and the corresponding decrease in the strain energy of transverse shear deformations are 5.8 and 3.3%. Thus, the rate of increase and decrease in W_i and W_s slows down with an increase in the aspect ratio. In Table 10, we have reported values of W for shells with R/a = 1 and 10 and different aspect ratios.

Table 10. Total strain energy of deformation, W (mJ), for spherical shells with different values of the aspect ratio.

R/a	1	2	3	4	5	6	7	8	9	10
a/h = 5	4580	4495	4468	4473	4478	4482	4485	4487	4488	4489
a/h = 10	6841	7622	8150	8434	8591	8684	8743	8783	8811	8831

3.4.3.1.2. *Effect of the shell curvature.* We have elucidated in Figure 17b for a spherical shell the effect of the normalized radius of curvature, R/a, for a/h = 5 and 10 on strain energies of the in-plane and the transverse deformations; their scales are shown on the right and the left vertical axes, respectively. It is found that the contribution to the total strain energy from the in-plane deformations increases and that from the transverse shear and the transverse normal deformations decreases with an increase in R/a. However, the increase in normalized value of W_i in going from R/a = 1 to R/a = 10 is only 2.9 and 4.3% for a/h = 10 and 5, respectively. The strain energy of transverse shear deformations is at most 6% for a/h = 5, 10 and the range of values of R/a considered. The contribution to the total strain energy from the transverse normal deformations is negligible as compared to those from other deformations for all configurations of the shell studied. In Table 11, we have listed for spherical shells with a/h = 5 and 10 values of W for different R/a ratios.

Table 11. Total strain energy of deformation, W (mJ), for spherical shells with different values of the radius of curvature.

a/h	2	3	4	5	6	7	8	9	10	12	14	16	18	20
R/a = 1	3149	3546	4074	4580	5026	5405	5722	5985	6205	6547	6808	7025	7222	7411
R/a = 10	1976	2798	3650	4510	5374	6237	7098	7956	8809	10,497	12,167	29,576	15,393	16,954

Table 12. Total strain energy of deformation, W (mJ), for doubly curved shells with different values of the ratio of the two radii of curvature.

R_2/R_1	2	3	4	5
a/h = 5	4941	4821	4748	4700
a/h = 10	8610	8949	9021	9026

3.4.3.1.3. *Effect of the curvature ratio.* In Figure 18, we have illustrated for the shell with $R_{1m}/a = 1$, and different values of $R_{2m} > R_{1m}$, the effect of the curvature ratio, R_{2m}/R_{1m}, on the strain energy of deformation due to the in-plane and the transverse deformations with their scales shown on the right and the left vertical axes, respectively. We note that the strain energy of in-plane deformations increases and that of transverse shear and transverse normal deformations decreases with an increase in value of R_{2m}/R_{1m}. For the range of R_{2m}/R_{1m} considered, the in-plane deformations account for at least 94.5% and the transverse shear deformations at most 5.8% of the total strain energy. The normalized value of W_i increases in going from $R_{2m}/R_{1m} = 1$ to $R_{2m}/R_{1m} = 10$ only by 2.6% for a/h = 5 and 10. The transverse normal deformations do not contribute noticeably to the total strain energy of the shell. In Table 12, we have listed values of W for doubly curved shells with $R_1/a = 1$, a/h = 5 and 10, and different R_2/R_1 ratios.

3.4.3.2. *Strain energies of stretching and bending deformations.*

3.4.3.2.1. *Effect of the shell curvature.* We have illustrated for a spherical shell in Figures 19a and 19b, the effect of the normalized radius of curvature, R/a, for a/h = 10 and 5, respectively, on strain energies of stretching and bending deformations. The results imply that the strain energy of bending deformations increases and that of stretching deformations decreases with an increase in the value of R/a. For a/h = 10, (W_{bend}, $W_{stretch}$) = (71.37%, 31.79%) of W for R/a = 1 and these values change to (95.93%, 4.17%) of W and (98.97%, 1.06%) of W for R/a = 5 and 10, respectively. Thus, the rate of increase and decrease in W_{bend} and $W_{stretch}$ slows down with an increase in the R/a ratio.

It is found that for R/a = 1 the contribution from transverse deformations to the total strain energy of bending deformations is at most 10.23 and 12.59% for aspect ratios of 10 and 5, respectively, which is small as compared to that from the in-plane deformations; these values decrease with an increase in the R/a ratio. Similarly, the contribution from $W_{stretch\text{-}tr}$ is negligible as compared to that from $W_{stretch\text{-}in}$ to the total strain energy of stretching deformations. The magnitude of the strain energy due

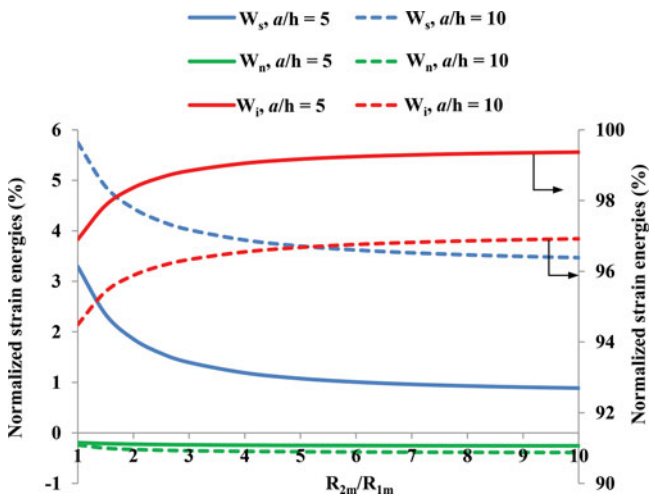

Figure 18. Variation with the curvature ratio, R_{2m}/R_{1m}, of normalized values of the strain energy due to in-plane, transverse shear, and transverse normal deformations for a monolithic cantilever doubly curved shell made of isotropic material and subjected to equal and opposite uniform tangential tractions on the outer and the inner surfaces. Plotted energies are normalized with respect to W (listed in Table 12) for each configuration of the shell.

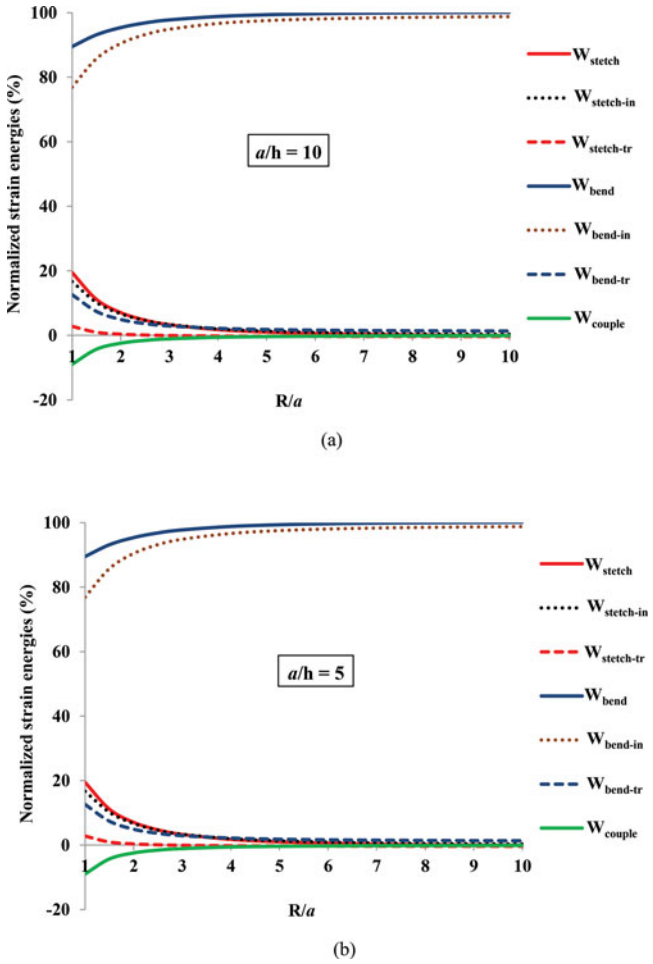

Figure 19. Variation with the normalized radius of curvature, R/a, of the normalized values of strain energies of stretching and bending deformations for an isotropic monolithic cantilever spherical shell with (a) a/h = 10, (b) a/h = 5, and subjected to equal and opposite uniform tangential tractions on the outer and the inner surfaces. Plotted energies are normalized with respect to W (listed in Table 10) for each configuration of the shell.

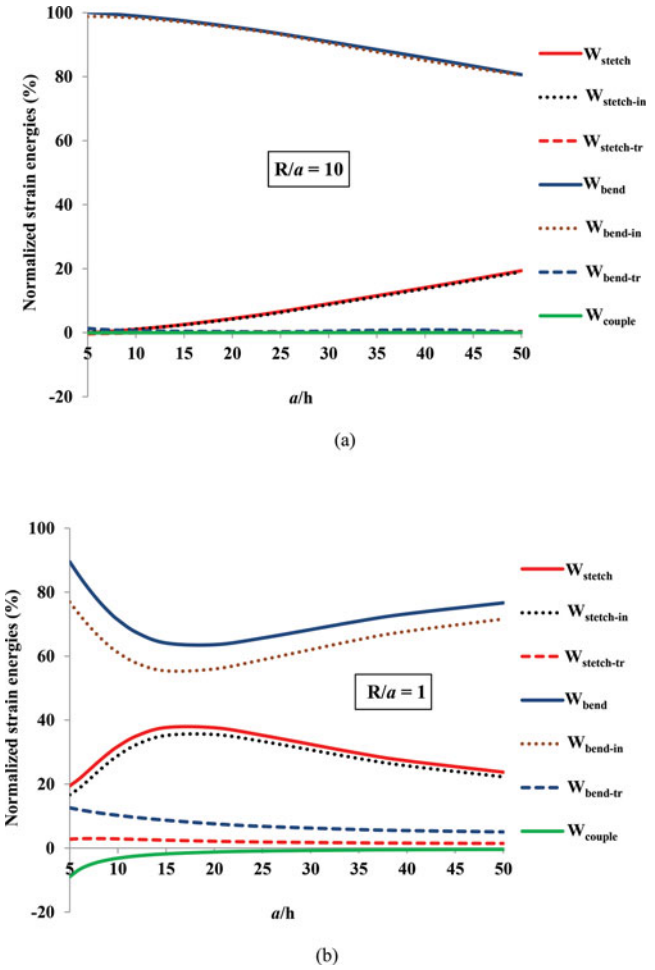

Figure 20. Variation with the aspect ratio, a/h, of the normalized values of strain energies due to stretching and bending deformations for an isotropic monolithic cantilever spherical shell with (a) R/a = 10, (b) R/a = 1, and subjected to equal and opposite uniform tangential tractions on the outer and the inner surfaces. Plotted energies are normalized with respect to W (listed in Table 11) for each configuration of the shell.

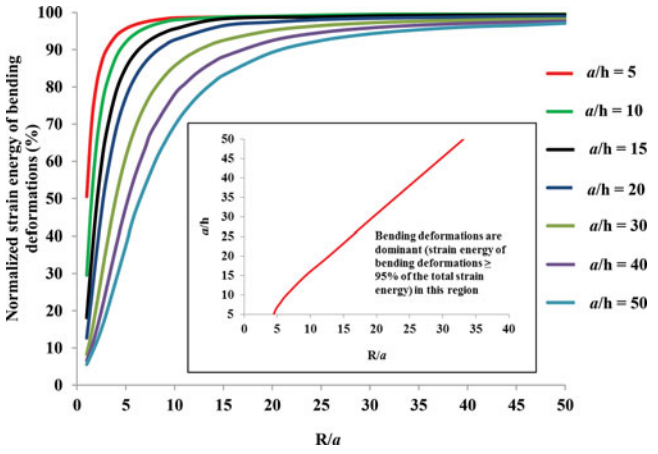

Figure 21. For different values of a/h, variation with the normalized radius of curvature, R/a, of the normalized values of strain energy due to bending deformations for a monolithic clamped spherical shell made of an isotropic linearly elastic material and subjected to a uniform normal tensile traction on the outer surface.

to interaction between stretching and bending deformations is 0.09W for R/a = 1 and a/h = 5.

3.4.3.2.2. *Effect of the aspect ratio.* We have exhibited in Figures 20a and 20b, the effect of the aspect ratio, a/h, on strain energies of stretching and bending deformations for a spherical shell with R/a = 10 and 1, respectively. It is found that strain energies of stretching (bending) deformations increase (decrease) with an increase in the aspect ratio for R/a = 10 with negligible contribution from transverse deformations. For R/a = 10, the total strain energy is due to bending deformations only when a/h = 5 and the contribution from W_{bend} to W reduces to 80.6% when a/h = 50. For a deeper shell with R/a = 1, W_{bend} ($W_{stretch}$) decreases (increases) for a/h ≤ 15 and increases (decreases) for a/h > 15 with an increase in the aspect ratio. For a/h = 15, the contribution to the total strain energy from bending and stretching deformations are 64.1 and 37.7%, respectively, with ($W_{bend\text{-}in}$, $W_{bend\text{-}tr}$) and ($W_{stretch\text{-}in}$, $W_{stretch\text{-}tr}$) = (0.554, 0.087)W and (0.352, 0.247)W, respectively.

3.4.3.2.3. *Shell geometries for dominant bending deformations.* For the problem studied in subsection 3.3.4.2, we have exhibited in Figure 21 the variation of the strain energy of bending deformations, W_{bend}, with the ratio, R/a, for different values of the aspect ratio, a/h. For a given value of a/h W_{bend} increases with an increase in R/a. However, the rate of increase in W_{bend}, and when it reaches the saturation value, strongly depend upon a/h. For example, for a/h = 5 W_{bend} exceeds 0.975 for R/a > 2 but for a/h = 50 W_{bend} exceeds 0.95 for R/a > 35. The inset is a phase plot of the region in the (R/a, a/h) space and shows that W_{bend} 0.95 for points below the red curve.

4. Conclusions

Static infinitesimal deformations of doubly curved shells made of either isotropic or orthotropic linear elastic materials have been studied using a third-order shear and normal deformable shell theory (TSNDT) and the finite element method (FEM). The effects of the shell aspect ratio, the ratio of the two radii of curvatures, and normal and tangential tractions applied on the shell major surfaces on strain energies of bending and stretching deformations have been quantified. For laminated shells, transverse shear and transverse normal stresses are computed using a one-step stress recovery scheme (SRS) and an equivalent single layer theory. No shear correction factor is used.

The transverse shear and the transverse normal stresses computed with the SRS are found to be close to those obtained by analyzing 3D deformations with the linear elasticity theory (LET). For a/h = 10 and R/a = 1, the centroidal deflection of a laminated shell predicted by the TSNDT agrees well with that obtained from the solution of the 3D LET equations with the difference between the two less than 3 and 7% for spherical and cylindrical shells, respectively. These differences decrease with a decrease in the shell curvature.

For shells made of an isotropic material the transverse shear stresses at points located in the vicinity of an edge (at a distance less than 5.5% edge-length) predicted by the TSNDT differ from the corresponding 3D LET solutions by ∼13% when they are obtained from constitutive relations. This difference reduces to ∼8% when the SRS is employed to find them. However, the in-plane axial stresses near an edge computed from the TSNDT differ by only 3% from the corresponding 3D LET solutions. The transverse normal stress computed from the constitutive relation and the TSNDT displacements differs from the applied

normal traction on the major surfaces by about 20% and does not exhibit the "boundary layer" phenomenon near the major surfaces as predicted by the 3D LET. However, when this stress is computed using the SRS the normal traction boundary conditions are satisfied with at most 3% error and the boundary layer effect is accurately captured. Similarly, for a cantilever shell subjected to equal and opposite tangential tractions on the two major surfaces, the transverse shear stress obtained directly from the constitutive relation differs from the applied tangential traction on a major surface near the clamped edge by about 14% which is reduced to 0.7% when the SRS is employed. For all problems studied, the one-step SRS gave accurate values of the transverse shear and the transverse normal stresses.

For a monolithic clamped spherical shell subjected to uniform normal traction on a major surface, the strain energy of in-plane deformations increases and that of transverse deformations decreases with an increase in either the aspect ratio (a/h) for a given radius of curvature R or the ratio R/a for a given a/h. For a thick shell with a/h = 5 and R/a = 10, the in-plane and the transverse deformations contribute nearly equally to the total strain energy. The strain energy of a shell almost equals that of a plate for R/a > 10. For a shell with R/a = 1 and a/h > 30, the strain energies of stretching deformations exceeds 90% of the total strain energy. However, for a shell with R/a = 10 and a/h < 20, the strain energy of bending deformations exceeds 90% of the total strain energy. For a shell with an aspect ratio of 10, the in-plane deformations contribute more as compared to the transverse deformations to the strain energy of bending deformations. However, for thick shells (a/h = 5), the in-plane and the transverse deformations contribute about equally to the strain energy of bending deformations.

For a monolithic cantilever spherical shell subjected to equal and opposite tangential tractions on the outer and the inner surfaces, transverse shear deformations contribute about 20% to the total strain energy of deformation for R/a = 1 and a/h = 2, and this contribution decreases with an increase in the aspect ratio. For R/a = 10, the shell deforms completely in bending with almost no stretching deformations when the aspect ratio equals 5. However, for a thin shell (a/h = 50), stretching deformations contribute ∼20% to the total strain energy.

The close agreement between results from the TSNDT and the 3D LET for a large variety of problems studied herein suggests that the TSNDT can be used to optimally design doubly curved shells subjected to generalized tractions.

Acknowledgment

RCB dedicates this article to his esteemed colleague and dear friend, Professor J. N. Reddy on his 70th birthday.

Funding

This work was partially supported by the Office of Naval Research Grant N00014-16-1-2309 to Virginia Polytechnic Institute and State University with Dr. Y. D. S. Rajapakse as the Program Manager. The views expressed in the article are those of the authors and neither of the funding agency nor of authors' institutions.

References

[1] M.S. Qatu, Vibration of Laminated Shells and Plates, Elsevier, Amsterdam, 2004.
[2] A.E.H. Love, Small free vibrations and deformations of thin elastic shells, Philos. Transs R. Soc. London, Ser. A, vol. 179, pp. 491–549, 1888.
[3] L.H. Donnell, Stability of thin-walled tubes under torsion, NACA Report 479, 1933.
[4] J.L. Sanders Jr., An improved first-approximation theory for thin shells, NASA Technical Report R-24, 1959.
[5] W. Flügge, Stresses in Shells, 2nd Edition, Springer, New York, 1973.
[6] K. Kraus, Thin Elastic Shells, Wiley, New York, 1967.
[7] E. Reissner, Small bending and stretching of sandwich type shells, National Advisory Committee for Aeronautics Technical Note No. 1832, 1947.
[8] S.S. Vel and R.C. Batra, The generalized plane strain deformations of thick anisotropic composite laminated plates, Int. J. Solids Struct., vol. 37, pp. 715–733, 2000.
[9] K.H. Lo, R.M. Christensen, and E.M. Wu, A high-order theory of plate deformation—Part 2: Laminated plates, J. Appl. Mech., vol. 44, no. 4, pp. 669–676, 1977.
[10] A.K. Murty, Higher order theory for vibrations of thick plates, AIAA J., vol. 15, no. 12, pp. 1823–1824, 1977.
[11] J.N. Reddy and C.F. Liu, A higher-order shear deformation theory of laminated elastic shells, Int. J. Eng. Sci., vol. 23, no. 3, pp. 319–330, 1985.
[12] K.M. Liew and C.W. Lim, A higher-order theory for vibration of doubly curved shallow shells, J. Appl. Mech., vol. 63, pp. 587–593, 1996.
[13] S. Xiao-Ping, An improved simple higher-order theory for laminated composite shells, Comput. Struct., vol. 60, no. 3, pp. 343–350, 1996.
[14] F.B. Hildebrand, E. Reissner, and G.B. Thomas, Notes on the foundations of the theory of small displacements of orthotropic shells, National Advisory Committee for Aeronautics, Washington, DC, 1949.
[15] E. Reissner, Stress-strain relations in the theory of thin elastic shells, J. Math. Phys., vol. 31, pp. 109–119, 1952.
[16] J.M. Whitney and C.T. Sun, Higher order theory for extensional motion of laminated composites, J. Sound Vib., vol. 30, no. 1, pp. 85–97, 1973.
[17] J.M. Whitney and C.T. Sun, A refined theory for laminated anisotropic cylindrical shells, J. Appl. Mech., vol. 41, no. 2, pp. 471–476, 1974.
[18] C.W. Bert, Analysis of shells. In: Analysis and Performance of Composites, L.J. Broutman, Ed., Wiley, New York, pp. 207–258, 1980.
[19] A.W. Leissa, Vibration of Shells, NASA SP-288, U.S. Government Printing Office, Washington DC, 1973.
[20] M.S. Qatu, E. Asadi, and W. Wang, Review of recent literature on static analyses of composite shells: 2000–2010, Open J. Compos. Mater., vol. 2, no. 3, pp. 61–86, 2012.
[21] K.M. Liew, C.W. Lim, and S. Kitipornchai, Vibration of shallow shells: A review with bibliography, Appl. Mech. Rev., vol. 50, no. 8, pp. 431–444, 1997.
[22] E. Carrera, Historical review of zig-zag theories for multilayered plates and shells, Appl. Mech. Rev., vol. 56, no. 3, pp. 287–308, 2003.
[23] S.A. Ambartsumian, Contributions to the theory of anisotropic layered shells, Appl. Mech. Rev., vol. 15, no. 4, pp. 245–249, 1962.
[24] S.A. Ambartsumian, Nontraditional theories of shells and plates, Appl. Mech. Rev., vol. 55, no. 5, pp. 35–44, 2002.
[25] J.N. Reddy, An evaluation of equivalent-single-layer and layerwise theories of composite laminates, Compos. Struct., vol. 25, no. 1–4, pp. 21–35, 1993.
[26] J.N. Reddy and R.A. Arciniega, Shear deformation plate and shell theories: From Stavsky to present, Mech. Adv. Mater. Struct., vol. 11, no. 6, pp. 535–582, 2004.
[27] R.K. Kapania, Review on the analysis of laminated shells, J. Press. Vessel Technol., vol. 111, pp. 88–96, 1989.
[28] K. Rohwer, S. Friedrichs, and C. Wehmeyer, Analyzing laminated structures from fibre-reinforced composite material—An assessment, Tech. Mech., vol. 25, no. 1, pp. 59–79, 2005.

[29] N.J. Pagano, Exact solutions for rectangular bidirectional composites and sandwich plates, J. Compos. Mater., vol. 4, no. 1, pp. 20–34, 1970.
[30] K. Rohwer, Application of higher order theories to the bending analysis of layered composite plates, Int. J. Solids Struct., vol. 29, no. 1, pp. 105–119, 1992.
[31] F. Tornabene, N. Fantuzzi, E. Viola, and R.C. Batra, Stress and strain recovery for functionally graded free-form and doubly-curved sandwich shells using higher-order equivalent single layer theory, Compos. Struct., vol. 119, pp. 67–89, 2015.
[32] A.K. Noor, W.S. Burton, and J.M. Peters, Predictor-corrector procedures for stress and free vibration analyses of multilayered composite plates and shells, Comput. Methods Appl. Mech. Eng., vol. 82, pp. 341–363, 1990.
[33] A.K. Noor, W.S. Burton, and J.M. Peters, Assessment of computational models for multilayered composite cylinders, Int. J. Solids Struct., vol. 27, no. 10, pp. 1269–1286, 1991.
[34] M. Malik and A.K. Noor, Accurate determination of transverse normal stresses in hybrid laminated panels subjected to electro-thermo-mechanical loadings, Int. J. Numer. Methods Eng., vol. 47, no. 1–3, pp. 477–495, 2000.
[35] T. Kant and K. Swaminathan, Estimation of transverse/interlaminar stresses in laminated composites—A selective review and survey of current developments, Compos. Struct., vol. 49, pp. 65–75, 2000.
[36] J.Q. Tarn and Y.M. Wang, An asymptotic theory for dynamic response of anisotropic inhomogeneous and laminated plates, Int. J. Solids Struct., vol. 31, no. 2, pp. 231–246, 1994.
[37] S. Vidoli and R.C. Batra, Derivation of plate and rod equations for a piezoelectric body from a mixed three-dimensional variational principle, J. Elast., vol. 59, no. 1–3, pp. 23–50, 2000.
[38] R.C. Batra and S. Vidoli, Higher-order piezoelectric plate theory derived from a three-dimensional variational principle, AIAA J., vol. 40, no. 1, pp. 91–104, 2002.
[39] L.F. Qian, R.C. Batra, and L.M. Chen, Free and forced vibrations of thick rectangular plates using higher-order shear and normal deformable plate theory and meshless Petrov-Galerkin (MLPG) method, Comput. Model. Eng. Sci., vol. 4, no. 5, pp. 519–534, 2003.
[40] R.C. Batra and S. Aimmanee, Vibrations of thick isotropic plates with higher order shear and normal deformable plate theories, Comput. Struct., vol. 83, no. 12, pp. 934–955, 2005.
[41] L.F. Qian and R.C. Batra, Transient thermoelastic deformations of a thick functionally graded plate, J. Therm. Stresses, vol. 27, no. 8, pp. 705–740, 2004.
[42] R.C. Batra and J. Xiao, Finite deformations of curved laminated St. Venant-Kirchhoff beam using layer-wise third order shear and normal deformable beam theory (TSNDT), Compos. Struct., vol. 97, pp. 147–161, 2013.
[43] P.H. Shah and R.C. Batra, Through-the-thickness stress distributions near edges of composite laminates using stress recovery scheme and third order shear and normal deformable theory, Compos. Struct., vol. 131, pp. 397–413, 2015.
[44] H. Shi, T. Yang, S. Jiang, W.L. Li, and Z. Liu, Curvature effects on the vibration characteristics of doubly curved shallow shells with general elastic edge restraints, Shock Vib., vol. 2015 pp. 1–15, 2015.
[45] J. Fan and J. Zhang, Analytical solutions for thick, doubly curved, laminated shells, J. Eng. Mech., vol. 118, no. 7, pp. 1338–1356, 1992.
[46] N.N. Huang, Influence of shear correction factors in the higher order shear deformation laminated shell theory, vol. 31, no. 9, pp. 1263–1277, 1994.
[47] C.P. Wu, J.Q. Tarn, and S.M. Chi, Three-dimensional analysis of doubly curved laminated shells, J. Eng. Mech., vol. 122, no. 5, pp. 391–401, 1996.
[48] C.R. Calladine, Theory of Shell Structures, Cambridge University Press, Cambridge, UK, 1989.
[49] A. Kalnins, Effect of bending on vibrations of spherical shells, J. Acoust. Soc. Am., vol. 36, no. 1, pp. 74–81, 1964.
[50] A.S. Saada, Elasticity: Theory and Applications, Pergamon Press, New York, 1974.
[51] C.A.M. Soares, C.M.M. Soares, and M.J. Freitas (Eds.), Mechanics of Composite Materials and Structures, Vol. 361, Springer Science & Business Media, Dordrecht 2013.

Appendix A

The matrices $\mathbf{Z_i}$ (i = 0, 1, 2, 3) and the operator matrix $\mathbf{L}$ appearing in Eq. (4) are given by Eqs. (A.1) and (A.2), respectively:

$$\mathbf{Z}_i = \begin{bmatrix} \frac{(y_3)^i}{H_1} & 0 & 0 & 0 & \frac{(y_3)^i}{R_1 H_1} & 0 & 0 & 0 \\ 0 & \frac{(y_3)^i}{H_2} & 0 & 0 & \frac{(y_3)^i}{R_2 H_2} & 0 & 0 & 0 \\ 0 & 0 & 0 & 0 & i\,x\,(y_3)^{i-1} & 0 & 0 & 0 \\ 0 & 0 & 0 & 0 & 0 & \frac{i\,(y_3)^{i-1} + (i-[\quad])(y_3)^i/R_2}{H_2} & 0 & \frac{(y_3)^i}{H_2} \\ 0 & 0 & 0 & 0 & 0 & 0 & \frac{[\quad](y_3)^{i-1} + (i-[\quad])(y_3)^i/R_1}{H_1} & \frac{(y_3)^i}{H_1} \\ 0 & 0 & \frac{(y_3)^i}{H_2} & \frac{(y_3)^i}{H_1} & 0 & 0 & 0 & 0 \end{bmatrix}, \tag{A.1}$$

$$\mathbf{L} = \begin{bmatrix} \frac{\partial}{\partial y_1} & 0 & 0 \\ 0 & \frac{\partial}{\partial y_2} & 0 \\ \frac{\partial}{\partial y_2} & 0 & 0 \\ 0 & \frac{\partial}{\partial y_1} & 0 \\ 0 & 0 & 1 \\ 0 & 1 & 0 \\ 1 & 0 & 0 \\ 0 & 0 & \frac{\partial}{\partial y_2} \\ 0 & 0 & \frac{\partial}{\partial y_1} \end{bmatrix}. \tag{A.2}$$

Appendix B

The derivation of equations governing static deformations of the shell using the principle of minimum potential energy based on the finite element (FE) formulation of the problem is presented in this section.

The equilibrium equations are derived from Eq. (B.1), which is obtained by substituting Eqs. (8.1) and (8.2) into Eq. (8) representing the principle of minimum potential energy:

$$\delta\Pi = \sum_{k=1}^{N} \int_{\Omega^k} \left(\delta\boldsymbol{\epsilon}^k\right)^{\mathrm{T}} \boldsymbol{\sigma}^k \, \mathrm{d}\Omega^k - \int_{\bar{\mathrm{A}}} \delta\mathbf{d}^{\mathrm{T}} \bar{\mathbf{f}} \, \mathrm{d}\bar{\mathrm{A}} = 0. \tag{B.1}$$

The nomenclatures of various terms in Eq. (B.1) are given in Section 2. We substitute in Eq. (B.1) for $\boldsymbol{\sigma}^k$ in terms of $\boldsymbol{\epsilon}^k$ from Eq. (7), and substitute for $\boldsymbol{\epsilon}^k$ in terms of the generalized displacements defined on the mid-surface of the shell from Eq. (4). Also, we substitute for $\mathbf{d}$ in terms of $\mathbf{d_i}$ (i = 0, 1, 2, 3) from Eq. (3). In the resulting expression for $\delta\Pi$, we integrate with respect to y_3 over the shell thickness to obtain the following integral equation:

$$\delta\Pi = \int_0^b \int_0^a \delta\mathbf{d}_\mathbf{i}^{\mathrm{T}} \mathbf{L}^{\mathrm{T}} \mathbf{D_{ij}} \mathbf{L} \mathbf{d_j} \, \mathrm{d}y_1 \mathrm{d}y_2 - \int_{\bar{\mathrm{A}}} \delta\mathbf{d}_\mathbf{i}^{\mathrm{T}} (y_3)^i \bar{\mathbf{f}} \, \mathrm{d}\bar{\mathrm{A}} = 0 \quad (\mathrm{i, j} = 0,\ 1,\ 2,\ 3), \tag{B.2}$$

where

$$\mathbf{D_{ij}} = \sum_{k=1}^{N} \int_{h_k}^{h_{k+1}} \mathbf{Z}_\mathbf{i}^{\mathrm{T}} \mathbf{C^k} \mathbf{Z_j} \, \mathbf{d}y_3. \tag{B.2.1}$$

We discretize the mid-surface, $\Re = [0,\ a] \times [0,\ b]$, of the shell into a FE mesh of $\mathrm{N_e}$ disjoint 8-node iso-parametric elements where the region $\Re_e$ occupied by the element e is given by, $\Re_\mathrm{e} = [y_1^e,\ y_1^{e+1}]\ \mathrm{x}\ [y_2^e,\ y_2^{e+1}]$. Thus, $\delta\Pi$ equals the sum of integrals over each element. The 12-dimensional vector $\bar{\mathbf{d}}$ of generalized displacements at a point in an element is expressed in terms of values of $\bar{\mathbf{d}}$ at the 8-nodes using the FE basis functions. The total number of unknowns in the problem equals $12\mathrm{N_{node}}$, where $\mathrm{N_{node}}$ = the number of nodes. We note that in the FE formulation of the corresponding 3D problem, the number of unknowns = $3\,\mathrm{N^*_{node}}$. Since $\mathrm{N^*_{node}} >> \mathrm{N_{node}}$, the total number of unknowns for the TSNDT is << than that for the 3D problem.

The degrees of freedom associated with the *i*th node are indicated by adding a superscript *i* to variables in Eq. (3.1). That is,

$$\mathbf{d_0^i} = \left[\mathrm{u_{10}^i}\ \mathrm{u_{20}^i}\ \mathrm{u_{30}^i}\right]^{\mathrm{T}},\ \mathbf{d_1^i} = \left[\mathrm{u_{11}^i}\ \mathrm{u_{21}^i}\ \mathrm{u_{31}^i}\right]^{\mathrm{T}},$$
$$\mathbf{d_2^i} = \left[\mathrm{u_{12}^i}\ \mathrm{u_{22}^i}\ \mathrm{u_{32}^i}\right]^{\mathrm{T}} \text{and}\ \mathbf{d_3^i} = \left[\mathrm{u_{13}^i}\ \mathrm{u_{23}^i}\ \mathrm{u_{33}^i}\right]^{\mathrm{T}}. \tag{B.3}$$

Thus, the vector of generalized variables $\mathbf{d_j}$ (j = 0, 1, 2, 3) of a point in an element e can be expressed in terms of the 24-D vector $\mathbf{d_j^e} = [\mathbf{d_j^1},\ \mathbf{d_j^2}, \ldots,\ \mathbf{d_j^8}]$ containing values of $\mathbf{d_j}$ at the 8-nodes of the element as follows:

$$\mathbf{d_j} = \boldsymbol{\Phi}\, \mathbf{d_j^e} \quad (\mathrm{j} = 0,\ 1,\ 2,\ 3), \tag{B.4}$$

where $\boldsymbol{\Phi}$ is a (3 × 24) matrix containing shape functions $(\psi_1,\ \psi_2, \ldots, \psi_8)$ associated with the 8 nodes of the element given by:

$$\boldsymbol{\Phi} = [\,\psi_1\mathbf{I} \quad \psi_2\mathbf{I} \ldots \quad \psi_8\mathbf{I}\,], \tag{B.4.1}$$

in which $\mathbf{I}$ is a (3 × 3) identity matrix.

Substituting for $\mathbf{d_m}$ ($m = 0,\ 1,\ 2,\ 3$) from Eq. (B.4) into Eq. (B.2), the first variation of the total potential energy of a typical element is given by:

$$\delta\Pi^e = \delta\mathbf{d_i^{e\mathrm{T}}}\, \mathbf{K_{ij}^e} \mathbf{d_j^e} - \delta\mathbf{d_i^{e\mathrm{T}}} (\mathbf{T_i^{+e}} + \mathbf{T_i^{-e}} + \mathbf{P_i^{+e}} + \mathbf{P_i^{-e}} + \mathbf{Q_i^{+e}} + \mathbf{Q_i^{-e}}) = 0 \quad (\mathrm{i, j} = 0,\ 1,\ 2,\ 3). \tag{B.5}$$

The elemental stiffness matrices $\mathbf{K_{ij}^e}$ and the elemental load vectors $\mathbf{T_i^{\pm e}}$, $\mathbf{P_i^{\pm e}}$, $\mathbf{Q_i^{\pm e}}$ (i, j = 0, 1, 2, 3) appearing in

Eq. (B.5) are given by:

$$\mathbf{K}_{\mathbf{ij}}^{\mathbf{e}} = \int_{y_2^e}^{y_2^{e+1}} \int_{y_1^e}^{y_1^{e+1}} \mathbf{B}^{\mathrm{T}}\mathbf{D}_{\mathbf{ij}}\mathbf{B}\, dy_1 dy_2, \text{ where } \mathbf{B} = \mathbf{L}\boldsymbol{\Phi}, \quad \text{(B.6)}$$

$$\mathbf{T}_{\mathbf{i}}^{\pm\mathbf{e}} = \int_{y_2^e}^{y_2^{e+1}} \int_{y_1^e}^{y_1^{e+1}} (y_3)^{\mathrm{i}}\boldsymbol{\Phi}^{\mathrm{T}}\mathbf{f}^{\pm} dy_1 dy_2,$$

$$\mathbf{P}_{\mathbf{i}}^{\pm\mathbf{e}} = \int_{y_2^e}^{y_2^{e+1}} \int_{-h/2}^{h/2} (y_3)^{\mathrm{i}}\boldsymbol{\Phi}^{\mathrm{T}}\mathbf{p}^{\pm} dy_3 dy_2,$$

$$\mathbf{Q}_{\mathbf{i}}^{\pm\mathbf{e}} = \int_{y_1^e}^{y_1^{e+1}} \int_{-h/2}^{h/2} (y_3)^{\mathrm{i}}\boldsymbol{\Phi}^{\mathrm{T}}\mathbf{q}^{\pm} dy_3 dy_1 \quad \text{(B.7)}$$

where $\mathbf{f}^+$ and $\mathbf{f}^-$ are the surface tractions prescribed on the outer and the inner surfaces, respectively; and $\mathbf{p}^+$, $\mathbf{p}^-$, $\mathbf{q}^+$, and $\mathbf{q}^-$ are the surface tractions prescribed on the edge surfaces, $y_1 = a$, $y_1 = 0$, $y_2 = b$, and $y_2 = 0$, respectively.

Recalling that variations in generalized displacements are arbitrary except at nodes where they are prescribed, we get the following equilibrium equations for a FE:

$$\mathbf{K}_{\mathbf{00}}^{\mathbf{e}}\mathbf{d}_{\mathbf{0}}^{\mathbf{e}} + \frac{1}{2}\left(\mathbf{K}_{\mathbf{01}}^{\mathbf{e}} + \mathbf{K}_{\mathbf{10}}^{\mathbf{e}\,T}\right)\mathbf{d}_{\mathbf{1}}^{\mathbf{e}} + \frac{1}{2}\left(\mathbf{K}_{\mathbf{02}}^{\mathbf{e}} + \mathbf{K}_{\mathbf{20}}^{\mathbf{e}\,T}\right)\mathbf{d}_{\mathbf{2}}^{\mathbf{e}} + \frac{1}{2}\left(\mathbf{K}_{\mathbf{03}}^{\mathbf{e}} + \mathbf{K}_{\mathbf{30}}^{\mathbf{e}\,T}\right)\mathbf{d}_{\mathbf{3}}^{\mathbf{e}} = \mathbf{F}_{\mathbf{0}}^{\mathbf{e}}$$

$$\frac{1}{2}\left(\mathbf{K}_{\mathbf{10}}^{\mathbf{e}} + \mathbf{K}_{\mathbf{01}}^{\mathbf{e}\,T}\right)\mathbf{d}_{\mathbf{0}}^{\mathbf{e}} + \mathbf{K}_{\mathbf{11}}^{\mathbf{e}}\mathbf{d}_{\mathbf{1}}^{\mathbf{e}} + \frac{1}{2}\left(\mathbf{K}_{\mathbf{12}}^{\mathbf{e}} + \mathbf{K}_{\mathbf{21}}^{\mathbf{e}\,T}\right)\mathbf{d}_{\mathbf{2}}^{\mathbf{e}} + \frac{1}{2}\left(\mathbf{K}_{\mathbf{13}}^{\mathbf{e}} + \mathbf{K}_{\mathbf{31}}^{\mathbf{e}\,T}\right)\mathbf{d}_{\mathbf{3}}^{\mathbf{e}} = \mathbf{F}_{\mathbf{1}}^{\mathbf{e}}$$

$$\frac{1}{2}\left(\mathbf{K}_{\mathbf{20}}^{\mathbf{e}} + \mathbf{K}_{\mathbf{02}}^{\mathbf{e}\,T}\right)\mathbf{d}_{\mathbf{0}}^{\mathbf{e}} + \frac{1}{2}\left(\mathbf{K}_{\mathbf{21}}^{\mathbf{e}} + \mathbf{K}_{\mathbf{12}}^{\mathbf{e}\,T}\right)\mathbf{d}_{\mathbf{1}}^{\mathbf{e}} + \mathbf{K}_{\mathbf{22}}^{\mathbf{e}}\mathbf{d}_{\mathbf{2}}^{\mathbf{e}} + \frac{1}{2}\left(\mathbf{K}_{\mathbf{23}}^{\mathbf{e}} + \mathbf{K}_{\mathbf{32}}^{\mathbf{e}\,T}\right)\mathbf{d}_{\mathbf{3}}^{\mathbf{e}} = \mathbf{F}_{\mathbf{2}}^{\mathbf{e}}$$

$$\frac{1}{2}\left(\mathbf{K}_{\mathbf{30}}^{\mathbf{e}} + \mathbf{K}_{\mathbf{03}}^{\mathbf{e}\,T}\right)\mathbf{d}_{\mathbf{0}}^{\mathbf{e}} + \frac{1}{2}\left(\mathbf{K}_{\mathbf{31}}^{\mathbf{e}} + \mathbf{K}_{\mathbf{13}}^{\mathbf{e}\,T}\right)\mathbf{d}_{\mathbf{1}}^{\mathbf{e}} + \frac{1}{2}\left(\mathbf{K}_{\mathbf{32}}^{\mathbf{e}} + \mathbf{K}_{\mathbf{23}}^{\mathbf{e}\,T}\right)\mathbf{d}_{\mathbf{2}}^{\mathbf{e}} + \mathbf{K}_{\mathbf{33}}^{\mathbf{e}}\mathbf{d}_{\mathbf{3}}^{\mathbf{e}} = \mathbf{F}_{\mathbf{3}}^{\mathbf{e}} \quad \text{(B.8)}$$

where

$$\mathbf{F}_{\mathbf{i}}^{\mathbf{e}} = \mathbf{T}_{\mathbf{i}}^{+\mathbf{e}} + \mathbf{T}_{\mathbf{i}}^{-\mathbf{e}} + \mathbf{P}_{\mathbf{i}}^{+\mathbf{e}} + \mathbf{P}_{\mathbf{i}}^{-\mathbf{e}} + \mathbf{Q}_{\mathbf{i}}^{+\mathbf{e}} + \mathbf{Q}_{\mathbf{i}}^{-\mathbf{e}} \ (\mathrm{i} = 0,\ 1,\ 2,\ 3). \quad \text{(B.8.1)}$$

Equations (B.8) are assembled using the standard technique to obtain:

$$\mathbf{KU} = \mathbf{F}, \quad \text{(B.9)}$$

where

$$\mathbf{K} = \begin{bmatrix} \mathbf{K}_{00} & \frac{1}{2}\left(\mathbf{K}_{01} + \mathbf{K}_{10}^{\mathrm{T}}\right) & \frac{1}{2}\left(\mathbf{K}_{02} + \mathbf{K}_{20}^{\mathrm{T}}\right) & \frac{1}{2}\left(\mathbf{K}_{03} + \mathbf{K}_{30}^{\mathrm{T}}\right) \\ \frac{1}{2}\left(\mathbf{K}_{10} + \mathbf{K}_{01}^{\mathrm{T}}\right) & \mathbf{K}_{11} & \frac{1}{2}\left(\mathbf{K}_{12} + \mathbf{K}_{21}^{\mathrm{T}}\right) & \frac{1}{2}\left(\mathbf{K}_{13} + \mathbf{K}_{31}^{\mathrm{T}}\right) \\ \frac{1}{2}\left(\mathbf{K}_{20} + \mathbf{K}_{02}^{\mathrm{T}}\right) & \frac{1}{2}\left(\mathbf{K}_{21} + \mathbf{K}_{12}^{\mathrm{T}}\right) & \mathbf{K}_{22} & \frac{1}{2}\left(\mathbf{K}_{23} + \mathbf{K}_{32}^{\mathrm{T}}\right) \\ \frac{1}{2}\left(\mathbf{K}_{30} + \mathbf{K}_{03}^{\mathrm{T}}\right) & \frac{1}{2}\left(\mathbf{K}_{31} + \mathbf{K}_{13}^{\mathrm{T}}\right) & \frac{1}{2}\left(\mathbf{K}_{32} + \mathbf{K}_{23}^{\mathrm{T}}\right) & \mathbf{K}_{33} \end{bmatrix}$$

$$\mathbf{U} = \begin{bmatrix} \mathbf{U}_0 \\ \mathbf{U}_1 \\ \mathbf{U}_2 \\ \mathbf{U}_3 \end{bmatrix}, \quad \mathbf{F} = \begin{bmatrix} \mathbf{F}_0 \\ \mathbf{F}_1 \\ \mathbf{F}_2 \\ \mathbf{F}_3 \end{bmatrix}, \quad \text{(B.10)}$$

in which $\mathbf{U_0}$, $\mathbf{U_1}$, $\mathbf{U_2}$, and $\mathbf{U_3}$ are the global vectors of generalized displacements, slopes, curvature, and curvature gradients, respectively.